university of groningen / faculty of science and engineering

On the acoustic transmitting behaviour of a waveguide sideloaded with cylindrical resonators.

Bachelor Research Project

Author:
L. H. Wendrich (S4483561)

Examiners:
dr. A.O. Krushynska
prof. dr. ir. P.R. Onck

Supervisor:
J. Hollewand

February 28, 2024

Abstract

In this thesis, the acoustic transmitting behaviour of a waveguide sideloaded with resonators is analysed using the transfer matrix method, the cost function and COMSOL. Comparisons are made between homogeneous systems, filled with water or air, and an inhomogeneous system that includes a volume of air in the resonator and water in the waveguide. Subsequently, the water-air ratio in the resonator and resonator separation distances are optimized to obtain maximum attenuation. This thesis has found that the inhomogeneous resonators serve as an effective low-frequency sound attenuator. Shifting the resonance frequencies to the lower frequency range (100-1000 Hz) and increasing its attenuating bandwidth, therefore achieving an average transmission of $\approx 0.08\%$ in this frequency range. The optimum water-air ratio in the resonator was found to be 100% air and the optimum waveguide lengths between resonators ($L_{2\rightarrow 10}$) for a 10 resonator system were found to be 0.02235 m, 0.1248 m, 0.1432 m, 0.1405 m, 0.1437 m, 0.1405 m, 0.1467 m, 0.1472 m and 0.0645 m respectively. The COMSOL model validated the analytical solution of the frequency responses but did show diminished correlation when the water-air ratio was altered from the evenly distributed configuration. To further investigate this, additional research is recommended.

Contents

1 Introduction

1.1 Metamaterials

To mitigate the excessive exposure of sound, different solutions are being applied today. The solutions which are especially interesting make use of specially designed materials that are able to manipulate the waves in more efficient ways than traditional materials are capable of. This kind of a material is called a metamaterial (MM). This term was firstly introduced by Roger Walser in 1999, deriving the word from the Greek word "$M\varepsilon\tau\alpha$", which means beyond [1]. The origin of the MM comes from research done by John Pendry and Victor Veselago who focused on the microwave range of electromagnetic waves. Later it was found that their techniques also seemed to be applicable on mechanical waves despite the difference in the physical nature of the two types of waves. The reason why this is possible originates from the similarities between the Maxwell and Helmholtz equations [1].

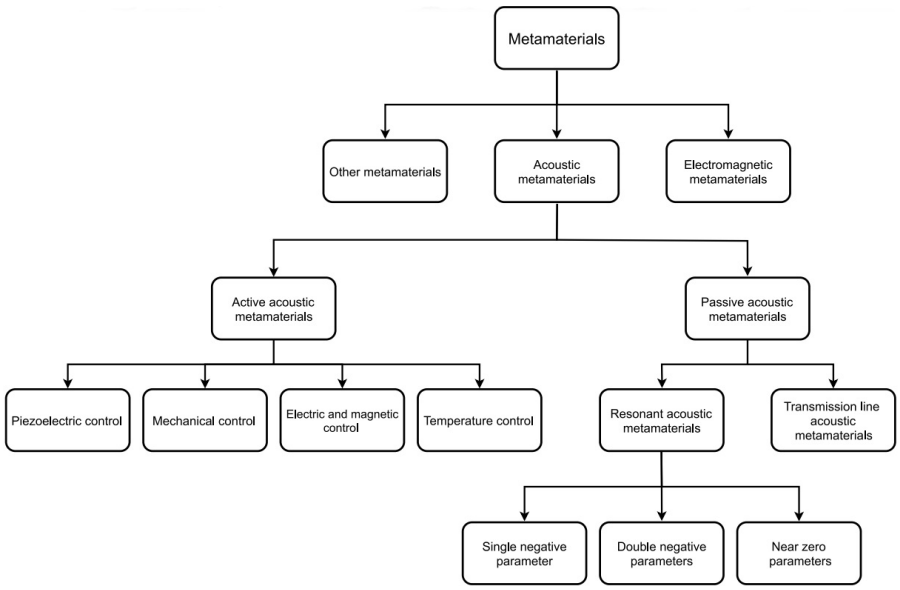

Figure 1: Classification diagram of metamaterials with the focus on acoustic metamaterials [1].

Utilizing these similarities, scientists found that the specially engineered materials for electromagnetic waves would have a similar effect on acoustic waves. The first proof of these acoustic metamaterials (AMMs) dates back to 2004 when Li and Chan conducted their research about a double-negative acoustic system [1]. Nowadays many different types of AMMs are used, categorized by their function, geometry and other features. Figure 1 presents a diagram visualising this classification.

An active AMM differs from a passive AMM through its possession of an external stimuli. This enables the AMM to alter its properties and therefore also its functionality. The stimuli can be activated through various control mechanisms. Passive AMM's can be subdivided into transmission line structures and those which contain resonating components. The transmission line AMMs uses materials as a waveguide to either transmit or produce sound, depending on the desired objective [2]. Resonant AMMs are again divided into three different subcategories, based on their disparity in parameters. These parameters can take single negative, double negative or near zero values. Usually the parameters of importance are the effective mass density and the effective bulk modulus. This can

cause an AMM to have properties like negative refraction, sound absorption or other unique acoustic behaviors [1].

1.2 Motivation

Nowadays many off-shore renewable energy sources are being constructed in Europe [3], with wind farms making up the majority of these sources [4]. When installing these wind farms, impact pile-driving procedures are used that generate very high intensity sound waves in the low frequency range. The frequencies that have the highest intensity are usually in the frequencies range from 10 Hz to 1000 Hz which coincides with the hearing ranges from many marine mammals [5]. This sound has the risk to induce lasting hearing damage or even total hearing loss while hearing is essential for many marine mammal's survival.

To mitigate this sound, various techniques are applied. One example currently uses an AMM in the form of cylindrical resonators. The geometry of these resonators are designed to have a natural frequency that matches the harmful frequencies encountered during pile driving, therefore attenuating the sound [6]. An image of a panel that consists out of these resonators can be found in Figure 2. The panel is depicted upside-down. When the panel is slowly submerged underwater, the resonators naturally encapsulate a volume of air. Therefore, an inhomogeneous acoustical system is created with water as the surrounding fluid and a ratio of water and air inside the resonators.

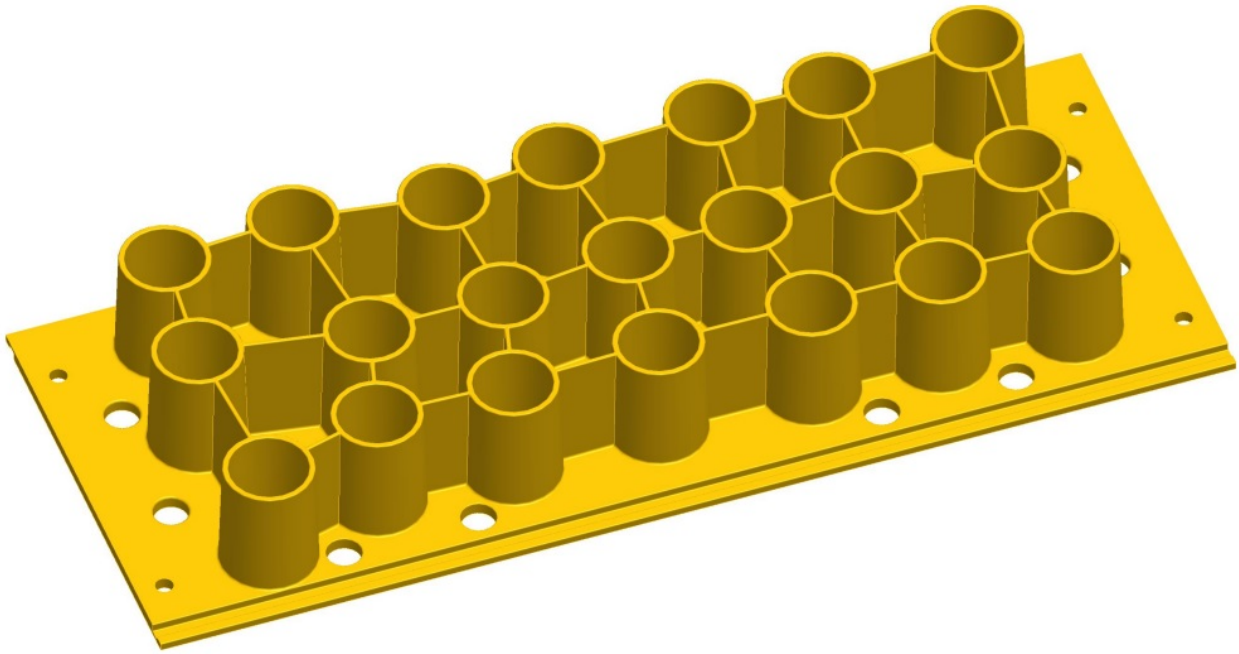

Figure 2: Resonant AMM used at 20-30 meters depth during pile-driving.

Upon observation, several questions arise. What is the difference in sound attenuation when the resonators are filled with water or air only (homogeneous)? And how does the air in the resonators influence this attenuation? In addition to this, the resonators are positioned in a specifically designed layout on the AMM panel. There could be various reasons for this, however, what would be the optimum configuration to ensure maximum attenuation?

1.2.1 Aim of the project

To answer the previously mentioned questions, the aim of this project is to analyse the acoustic behaviour of the resonators in a homogeneous and inhomogeneous case. This is done by using a simplified, one dimensional model that consists out of a waveguide and a linear array of sideloaded resonators. Using this model, this project also aims to find the optimum distances between the resonators for an inhomogeneous system. Both objectives are investigated through analytical calculations, utilizing the transfer matrix method (TMM) and the cost function. The systems are analyzed in the frequency range of 100-1000 Hz through the transmission coefficients and transmission loss. This will be done for different amount of resonators, separation distances and water-air ratios. The water-air ratio and resonators separation will be optimized utilising a maximum of three distinct methods. The optimum resonator separations will be further investigated using models made through COMSOL using Pressure Acoustics, Frequency Domain (acpr) from the acoustic module. The frequency response of both the analytical and COMSOL solutions will be compared.

For the homogeneous systems, it is expected to show high transmission up till its resonance frequency where a short but high intensity dip in transmission will occur. The inhomogeneous system is expected to show similar response, however, with a lower resonance frequency. Regarding the optimization, a non-periodic configuration is predicted to obtain better attenuation as in this way, the configuration is more likely to be suitable for a broader variety of frequencies. Lastly, the volume of air in the resonator in the inhomogeneous system is expected to lower the resonance frequency, as the speed of sound in air is less than a quarter than the speed of sound in water.

This research aims to benefit the current use and development of resonant AMMs in underwater environments and create a deeper understanding on inhomogeneously filled resonators.

2 Background Literature

Several physical principles are applied in this thesis to develop and analyze the model. To offer some theoretical perspective, the most significant principles that support the findings are discussed in this section.

2.1 Sound propagation

When sound is traveling without obstruction through a medium it usually dissipates exponentially. This decay is dependent on the characteristic properties of the medium. With an initial amplitude of A_0, this dependency will have the following form [7]

$$A(x) = A_0 e^{-\mu x}. \tag{1}$$

Here x denotes the distance travelled and μ represents the propagation constant. This consists out of a real and imaginary part which can be denoted as $\mu = \alpha + j\beta$. The imaginary component is known as the phase constant and the real part is known as the attenuation constant. In this context, the symbol μ can be understood as the MMs effective wavenumber (k). Waves can travel in frequency bands where μ is imaginary. Attenuation happens in band gaps or frequency values that give rise to a real part of μ. This real component defines the degree of attenuation of waves that are transmitted. [8].

The acoustic pressure (p) and displacement vector ($\mathbf{u}$) of plane waves in unbounded fluids moving in the z direction are expressed as [9]

$$\begin{aligned} p(z,t) &= A \exp j\omega(t - kz), \\ \mathbf{u} &= \left(0, 0, \frac{-jAk}{\rho\omega^2} \exp j\omega(t - kz)\right). \end{aligned} \tag{2}$$

Pressure and velocity are therefore related through

$$p(z,t) = Z \cdot v_z, \tag{3}$$

where Z represents the acoustic impedance of the fluid. This serves as the resistance of a medium to a longitudinal wave motion and describes the connection between the sound pressure that is acting and the resulting particle velocity [10]. It is analogous to electrical impedance which is also known as the electrical resistance. When waves are discussed that propagate through confined mediums, the acoustic impedance is defined as

$$Z = \frac{\rho c}{S}. \tag{4}$$

Here ρ is the fluid density, S the cross sectional area of the confinement and c is the speed of sound in the medium. When the propagating sound encounters a change in material or substance, the behaviour of the wave is dependent on the similarity between the two impedance's. Large impedance variations result in a significant percentage of the wave being reflected. Accordingly, the transmission and reflection coefficients are defined as follows [11] [12]:

$$T = \frac{2Z_1}{Z_1 + Z_2},$$
$$R = \frac{Z_1 - Z_2}{Z_1 + Z_2}. \tag{5}$$

2.2 Sound Attenuation

Various methods can be used to attenuate sound. In order to mitigate sound waves, they can first be scattered/reflected using for example the impedance mismatch. If, however, the scattering of waves is undesired, the sound must be attenuated using absorption. Sound absorption happens through various approaches; viscous losses, the use of resonators, vortex shedding, thermal elastic damping, and direct mechanical damping from the material itself are some examples. [10]

To accomplish more effective sound attenuation as opposed to the regular dissipation, viscous effects are maximized. In regular absorption panels, this is done by using porous materials. Because of their cellular and less dense structure, the surface area where viscothermal effects occur is optimized [10].

2.3 Resonators

In resonators, viscous friction inside the resonator causes sound absorption. Resonators are geometries designed to selectively amplify or attenuate specific frequencies of sound. When the frequency of the sound wave matches the natural frequency of the resonator, resonance occurs. In addition to the absorption through thermal viscous effects, resonators radiate sound waves from their opening, causing it to serve as a sound source. This enhances the sound-attenuating qualities through resonance-based destructive interference [13]. Although there exists a great variety of acoustical resonators, the two that are most widely used are the Helmholtz resonator and the quarter-wave tube.

The geometry of a Helmholtz resonator, named after the German physicist Hermann von Helmholtz [14], consists of a neck and a cavity. During resonance, the fluid in the neck vibrates, being pushed inwards by oncoming waves and outwards by the opposing pressure that the compressed fluid in the cavity is providing. This resonator is therefore approximated as a mass-spring system, the mass consisting out of the fluid volume occupying the neck and the spring consisting out of the compressed fluid volume in the cavity. To calculate the natural-frequency of this resonator, the following equation is used [15]

$$f_r = \frac{c}{2\pi}\sqrt{\frac{S}{LV}}. \tag{6}$$

S representing the cross-sectional area of the resonators opening, L the length of the neck and V the volume of the cavity. The second type of a resonator is a quarter-wave tube. This can be seen as a simple side branch, having a constant cross-sectional area. The resonator shows resonance at [15]

$$f_r = \frac{nc}{4L}. \tag{7}$$

With n referring to the order of the resonance. Reflected waves that destructively interfere and viscothermal effects cause absorption in this resonator as well.

2.4 Physical System

As previously mentioned, a basic model is developed in order to analyse the attenuating characteristics of the resonators. This section will describe how this is approached.

2.4.1 The waveguide

To start off, a wave guide has to be correctly approximated. When a plane wave enters the waveguide, the no-slip condition at the walls alters the flow profile. This effect can be seen in Figure 3 below.

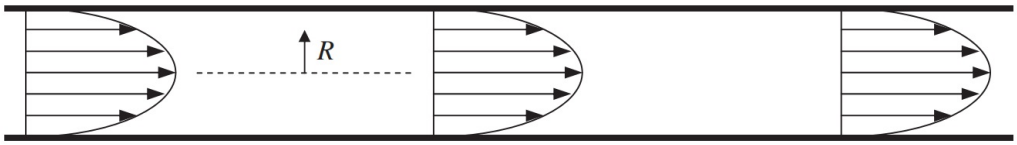

Figure 3: Flow profile in a cylindrical tube. [16]

To model closer to the real scenario, the waves in the waveguide are considered as plane waves. Viscous effects therefore need to be neglected. To allow for this approximation, the viscous boundary layer thickness $\delta = \sqrt{2\eta/\rho\omega}$ has to be much smaller than one ($\delta << 1$). The allowed frequency range therefore becomes

$$\frac{2\eta}{\pi\rho d^2} << f < \frac{c}{2d}, \tag{8}$$

where η is the dynamic viscosity coefficient, ω the angular frequency and d the waveguide's diameter [7].

2.4.2 The resonators

The resonators are sideloaded to the waveguide as depicted in Figure 4. The focus on the low frequency range allows for the simpler approximation of the resonators geometry that considers the resonators to be perfect cylinders. At lower frequencies, the volume becomes the primary factor influencing the resonance frequency. [8].

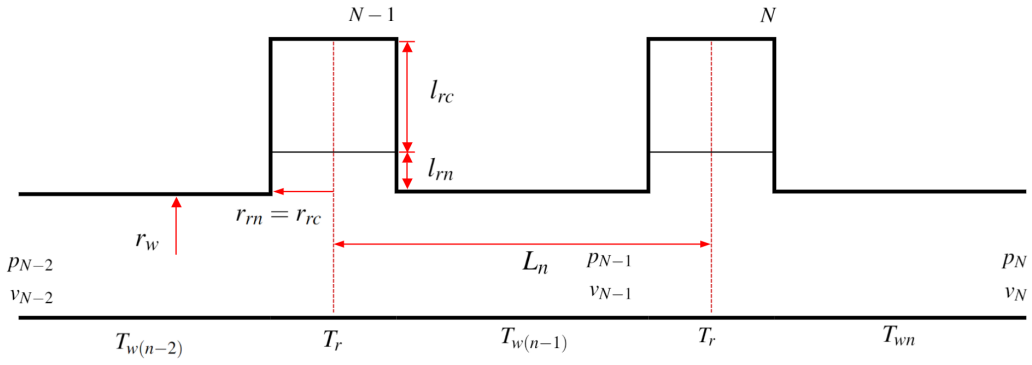

Figure 4: Schematic of the waveguide with sideloaded resonators.

2.4.3 Wavenumber and impedance

To compare the analytical results with the results obtained through COMSOL, the viscous losses need to be included for the waveguide. Therefore, the equations describing the wavenumber and characteristic impedance are altered to include complex values and therefore attenuation.

$$k_i = \frac{\omega}{c}(1+\frac{(1-j)\delta}{r_i\sqrt{2}}(1+(\gamma-1)\sqrt{P_r})),$$
$$Z_i = \frac{\rho c}{S_i}(1+\frac{(1-j)\delta}{r_i\sqrt{2}}(1-(\gamma-1)\sqrt{P_r})). \tag{9}$$

Where the subscript i denotes the geometry under consideration. $i = w$ refers to the waveguide, $i = rn$ to the resonators neck and $i = rc$ represents the resonators cavity. When the system is homogeneous, $Z_{rn} = Z_{rc}$ and $k_{rn} = k_{rc}$. However, when the resonator is partially filled with water and air, Z_{rn} will represent the water filled part and Z_{rc} the part of the resonator that includes air. γ and P_r represent the heat capacity ratio and Prandtl number respectively [17] [18] and will be taken as $\gamma = 1.4$ and $P_r = 0.71$ in air and $\gamma = 1.330$ and $P_r = 7.0$ in water.

2.5 Transfer Matrix Method

The aforementioned waveguide can be approximated as an one-dimensional system. Therefore, to analyse the transmittance, the transfer matrix method (TMM) can be used. This method is also applied in the one-dimensional wave analysis of quantum particles, electromagnetic and elastic waves [19].

The TMM's core concept is the division of the system into pieces. There is a transfer matrix for every fragment that describes its characteristic behaviour. Simple continuity conditions can be used to regulate the transitions using transfer matrices. This makes it possible to utilise matrix multiplication to ascertain, from the wave's initial conditions alone, its final properties. The transfer matrix in a system of length L relates the initial sound pressure p and normal acoustic velocity v to its ultimate values mathematically through

$$\begin{bmatrix} p \\ v \end{bmatrix}\Big|_{x=0} = \mathbf{T}\begin{bmatrix} p \\ v \end{bmatrix}\Big|_{x=L}. \tag{10}$$

$\mathbf{T}$ in this description stands for the transfer matrix and is derived using the following equation containing N resonators:

$$\mathbf{T} = \begin{bmatrix} T_{11} & T_{12} \\ T_{21} & T_{22} \end{bmatrix} = \prod (T_{wn}T_r)^{N-1}T_{wn}. \tag{11}$$

T_{wn} and T_r corresponding to the transfer matrices of the waveguide, having a length L_n, and resonator respectively. n refers to the nth T_{wn}. The formation of these matrices is as follows [17] [18] [20]:

$$T_{wn} = \begin{bmatrix} cos(kL_n) & jZ_w sin(kL_n) \\ \frac{j}{Z_w} sin(kL_n) & cos(kL_n) \end{bmatrix}, \tag{12}$$

$$T_r = \begin{bmatrix} 1 & 0 \\ \frac{1}{Z_r} & 1 \end{bmatrix}. \tag{13}$$

The impedance of the resonant element Z_r is also obtained using the TMM. This can be derived using equation 12, with L_n now representing the length of the neck and cavity (l_{rn} or l_{rc} respectively) of the resonator. Next to this, an additional transfer matrix is used to captivate the length correction of the resonator due to the discontinuity from the neck to the waveguide. This matrix is formulated as follows [20]:

$$T_{\Delta l} = \begin{bmatrix} 1 & jZ_{rn}k_{rn}\Delta l \\ 0 & 1 \end{bmatrix}. \tag{14}$$

with Δl representing the length correction as [20]

$$\Delta l = 0.82(1 - 0.235\frac{r_{rn}}{r_w} - 1.32(\frac{r_{rn}}{r_w})^2 + 1.54(\frac{r_{rn}}{r_w})^3 - 0.86(\frac{r_{rn}}{r_w})^4)r_{rn} \tag{15}$$

Combining these matrices through $T = T_{rn}T_{\Delta l}T_{rc}$, the resonators impedance (Z_r) can be derived as the following [20]:

$$Z_r = -j\frac{cos(k_{rn}l_{rn})cos(k_{rc}l_{rc}) - (\frac{Z_{rn}}{Z_{rc}})k_{rn}\Delta l\cos(k_{rn}l_{rn})\sin(k_{rc}l_{rc}) - (\frac{Z_{rn}}{Z_{rc}})\sin(k_{rn}l_{rn})\sin(k_{rc}l_{rc})}{\sin(k_{rn}l_{rn})\cos(k_{rc}l_{rc})/Z_{rn} - k_{rn}\Delta l\sin(k_{rn}l_{rn})\sin(k_{rc}l_{rc})/Z_{rc} + \cos(k_{rn}l_{rn})\sin(k_{rc}l_{rc})/Z_{rc}}. \tag{16}$$

Now using the transfer matrices from equations 12 and 13, complemented by the impedances and wavenumbers from equations 9 and 16 the transfer matrix **T** can be computed. Consequently, the complex transmission, reflection and absorption coefficients are obtained using the formula below [18]

$$t = \frac{2}{T_{11} + T_{12}/Z_w + T_{21}Z_w + T_{22}},$$

$$r = \frac{T_{11} + T_{12}/Z_w - T_{21}Z_w - T_{22}}{T_{11} + T_{12}/Z_w + T_{21}Z_w + T_{22}}, \tag{17}$$

$$\alpha = 1 - |t|^2 - |r|^2.$$

Based on this, the transmittance of sound waves can be estimated for different frequencies. Consequently, the transmission loss (TL) can be computed as

$$TL = 20log_{10}(t^{-1}) \quad [dB]. \tag{18}$$

2.6 Optimization

For optimization, a cost function is formulated. This function, which calculates the average difference between the desired and actual result, appears as follows

$$J = \frac{1}{m}\sum_{i=1}^{m}|t_0 - t| = \frac{1}{m}\sum_{i=1}^{m}t. \tag{19}$$

Where m denotes the number of frequencies that are being evaluated, t_0 the desired transmission coefficient which is in this case 0% and t the obtained transmission coefficient.

3 Simulation/Modeling

The theory previously discussed is implemented through various models. This section will cover the techniques applied in these models.

3.1 Assumptions

To simplify the real life scenario multiple assumptions had to be made. The main reasons for this being the complexity of the system and time constraints.

Firstly, the sound waves are defined as ideal plane waves. The waves that encounter the resonators in the real scenario are however not perfect planes. Secondly, the system is defined to have sound hard boundaries, meaning that no energy can leave the system. The resonators in question are constructed out of a plastic material that does in fact allow for transmission. Next to this, the system is assumed to be perfectly stationary, therefore making internal vibrations of the structure impossible which is not the case in real life as well. Lastly, no higher pressures and densities are used for the fluids. This deviates from the real physical system that is lowered into water. Causing especially the density of air to increase.

The resonant AMM depicted in Figure 2 comes in different shapes and sizes to account for the decreased volume of air at greater depths. The models in this report will however only analyses the frequency responses of the smallest resonator used in the shallowest waters ranging up to 20 meters in depth to minimize the impact of the increased density of air. The radius and length of this resonator are 11.176 cm and 43.7 cm respectively. Larger resonators however are expected to show similar responses, with the difference in geometry causing a shift in the resonance frequency.

During all modeling, a density of 1.293 kg/m^3 for air and 998 kg/m^3 for water was used. The speed of sound was taken to be 343 m/s and 1461 m/s for air and water respectively.

3.2 Python

Using python, the TMM is implemented over frequency range of 100 - 2000 Hz. The frequencies below 100 Hz are not included in the analysis as these frequencies are too low for the formulas to portray accurate results. Additionally, the effect of the waveguides radius and L_1 and L_n is investigated. If this effect appears to not be significant, they are set as constants. Afterwards, the code is firstly checked for the homogeneous case with $N = 0, 1$ and compared to its theoretical frequency response characterized by

$$t_0 = \frac{1}{e^{ik_wL}}, \tag{20}$$

$$t_1 = \frac{2}{2jsin(k_wL)cos(k_wL)(\frac{Z_w}{Z_r}+2)+(cos^2(k_wL)-sin^2(k_wL))(\frac{Z_w}{Z_r}+2)}. \tag{21}$$

As can be seen from equation 21, the transmittance becomes highly dependent on the impedance ratio Z_w/Z_r when resonators are added. After the theoretical result matches the results obtained through python, more resonators are added to the system. For the inhomogeneous system, a neck and cavity length have to be determined to represent the water-air ratio. This ratio was firstly set to a 50/50 ratio, to be optimized later on in the process. The resulting transmission coefficient and transmission loss

can then be compared to literature. If the results obtained are similar, the code is operating correctly. Consequently, the optimizing can begin.

3.2.1 Optimizing l_{rn}/l_{rc}

This step will consist out of optimizing the water-air ratio for $N = 1$. The cost function in combination with t will be used to analyse the transmitting behaviour in the chosen frequency range for every water-air ratio. The ratio will range from 0-100% air, starting at 0% and increasing in steps of 1%. The ratio that corresponds to the lowest value of J will be used as the fixed water-air ratio in further simulations. After this is found this value will be compared with systems that include more resonators. If this appears to be similar the ratio will be set constant.

3.2.2 First optimization method for L_n

If the first and last transfer matrix of the waveguide do not have an considerable effect on the wave-field, they do not have to be optimized. Therefore, the first optimization method starts with a two resonator system. The same approach will be used as when optimizing l_{rn}/l_{rc}. The value of L_2 that causes the minimum cost function will be obtained and afterwards set fixed in the next configuration. This next configuration will now include three resonators. L_3 will now be determined in the same way and set constant. This continues until all intermediate distances are optimized. The range for which L_n is optimized will lay between $2r_n$ and 1 m. Greater distances are not taken into consideration since these lay out of the focus of this thesis.

3.2.3 Second optimization method for L_n

After the first optimization is done, the total optimized configuration is again analysed. Now each resonator is moved from its position, confined by the other resonators in their previously determined positions. The total length of the waveguide will therefore be kept constant. The optimization will be done once systematically, starting with L_2 and ending with $L_{(n-1)}$, and once in reverse order.

3.2.4 Third optimization method for L_n

To assess the quality of the previously mentioned optimization methods, a third method will be applied. This method will generate random lengths for all waveguides under consideration and calculate the corresponding value for J of the system. Certain constraints will be used to make sure the resonators do not overlap each other. The configuration that obtains the lowest value for J will be optimized using the second optimization method. Consequently, the lowest value obtained in that step will optimized again. However, this time it will be done dynamically using the `scipy.optimize.minimize` module from python, using the previously obtained configuration as the initial guess.

3.3 COMSOL

The next step was to analyse the configuration obtained through the third optimization method using the Finite Element Method (FEM). For this the Pressure Acoustics, Frequency Domain was used out of the Acoustic module to solve for the acoustic problem. Due to my inexperience with COMSOL, the model ”Helmholtz Resonator with Porous Layer” [21] appeared to be of great help for the foundation of this model.

The pressure acoustics in the waveguide, resonator neck and resonator cavity are defined using the effective wavenumber and characteristic impedance from Equation 9, each containing the characteristics of its operating medium. For visualisation of the model, Figure 5 shows the cavity in green and the neck coloured in blue. The lengths of these parameters are altered during the optimization process. To ensure that the wave field at the inlet and outlet is not directly influenced by the resonator, an extra 0.3 m is added.

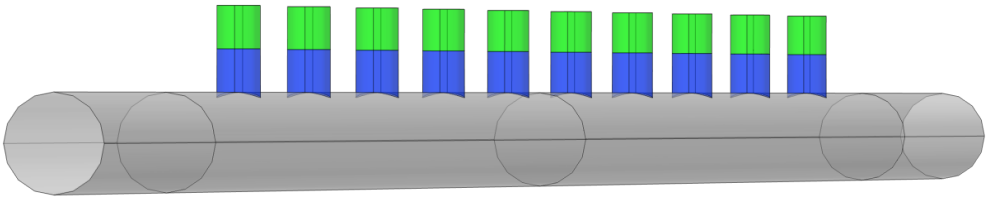

Figure 5: Schematic of the periodic configuration with the resonator neck and cavity coloured in blue and green respectively.

After the geometry and acoustic pressure is set-up, a plane wave is defined to enter the waveguide. For this, the Port boundary condition is applied. This boundary condition is specially designed to excite and absorb sound waves as they enter or exit a waveguide of various shapes. One port therefore has to be defined at the inlet with an amplitude which in this model will be set to 1, and one port at the outlet without initial excitement. The azimuthal and radial mode numbers both have to be set to 0 at both ports to define the plane wave. Utilizing both ports, the total acoustic field can be denoted as

$$p_t = \sum_{i \in bnd} A_{in} e^{i\phi} (S_{ij} + \delta_{ij}) p_i, \tag{22}$$

where p_t represents the total pressure, i the summation at the given boundary over all ports, A_{in} the initial amplitude at port j, ϕ the phase of the incident field, S_{ij} the scattering parameter, p_i the shape of the mode at port i. From the scattering parameters, the transmission (S_{11}), reflection (S_{21}) and absorption coefficient can be immediately calculated [22].

4 Results

In this section, the findings of the analytical and FEM model will be displayed and critically analysed.

4.1 Analytical results

To start off, the waveguide's diameter had to be determined. Using equation 8, this value was known to be in the range of 0.8 mm << d < 375 mm. In this range, various diameters were tested in a system using only 1 resonator. The results can be found below.

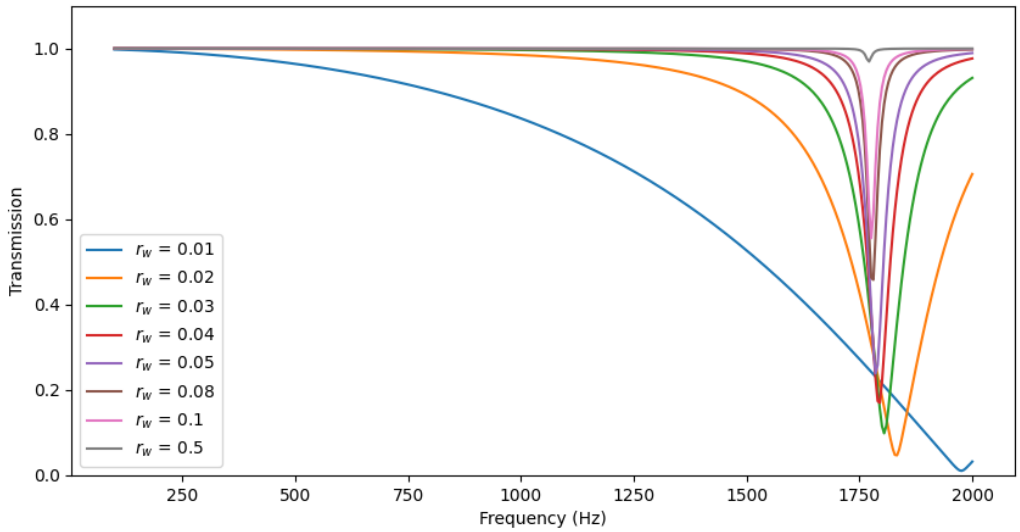

Figure 6: 1 resonator system with increasing r_w (m) for an air filled system that includes losses.

As can be seen, with every centimeter the radius is decreased, the intensity of the peak decreases as well. The same occurred when using water as the homogeneous medium or when using the inhomogeneous system. To still obtain clear and visible results, the chosen diameter was therefore chosen to be 0.10 m.

Afterwards, the effect of the first and last transfer matrix were analysed in all three cases. The analyses all showed similar results. For air, the results are shown in Figure 7. From this it can be concluded that next to viscous losses, these lengths does not have an effect on the results. Therefore, the first and last transfer matrices (T_{w1} and T_{wn}) do not need to be included in the optimization method and are assigned the fixed length of 0.2 m.

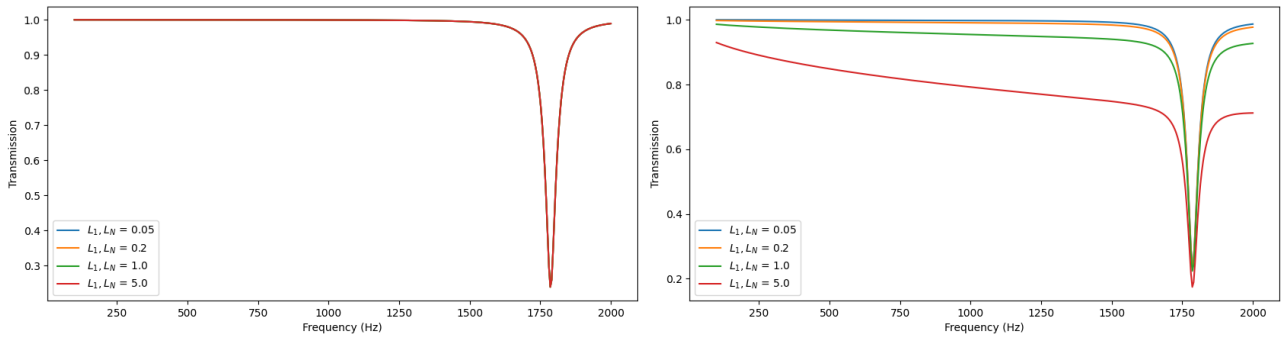

(a) (b)

Figure 7: 1 resonator system in air with increasing L_1 and L_n (m) for (a) the lossless case and (b) the case that includes losses.

The last dimension that needs to be determined is the water-air ratio in the resonator for the inhomogeneous case. When the resonators are submerged underwater, parts of the air escapes the encapsulation. Furthermore the air gets compressed. Therefore, the neck and cavity length will first be set equal, meaning that the resonator is filled with water for 50% and with air for the other 50%. The effect of this ratio on the transmission coefficient will later be analysed and optimized.

4.1.1 Frequency responses

With r_w, L_1, L_n and l_{rn}/l_{rc} now having fixed values, the only dimension that is missing is the value for L_n. Because no optimization can be done yet, this value will first take the constant value of 0.2 m. Later on this will be changed to its optimum values. Evidently, the frequency responses for the homogeneous and inhomogeneous cases could be obtained. The results that only consider losses in the resonators can be found below. The expected resonance frequency of the resonator was found at 1962 Hz and 8358 Hz in air and water using Equation 2.3.

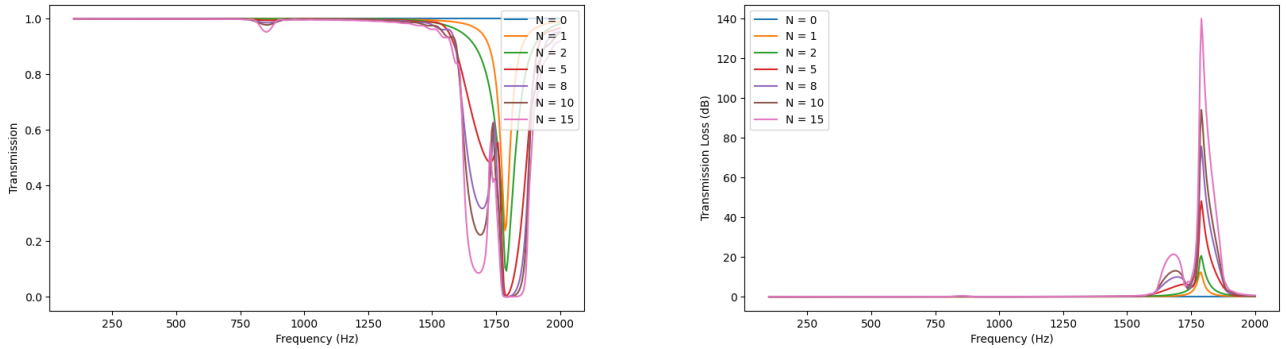

Figure 8: Frequency response for an air filled system with different number of resonators.

Firstly we will compare Figure 8 and 9. These responses look very alike, with each peak also occurring around the expected resonance frequency. Next to this, a small peak occurs before the resonance frequency. In water, this peak is a greater distance apart from the expected resonance frequency.

When comparing the inhomogeneous case depicted in Figure 10 to the homogeneous cases, an interesting difference can be observed. The water-air filled resonators cause the resonance frequencies

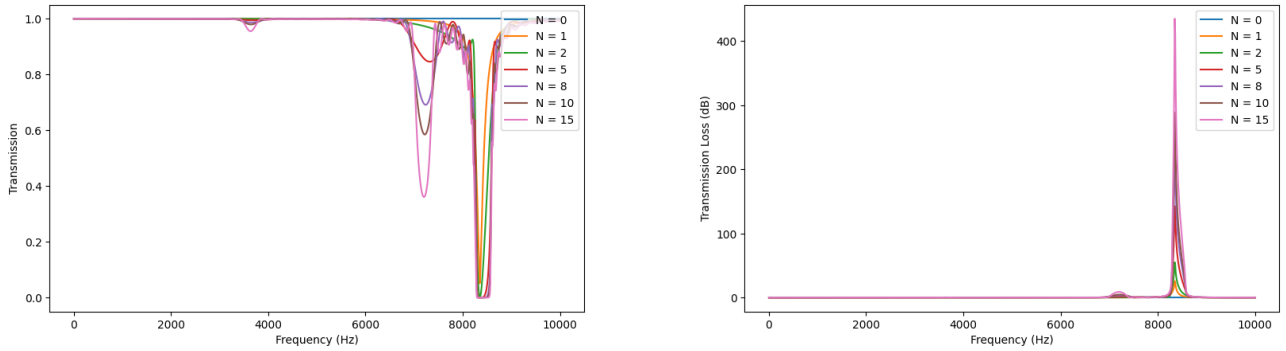

Figure 9: Frequency response for a water filled system with different number of resonators.

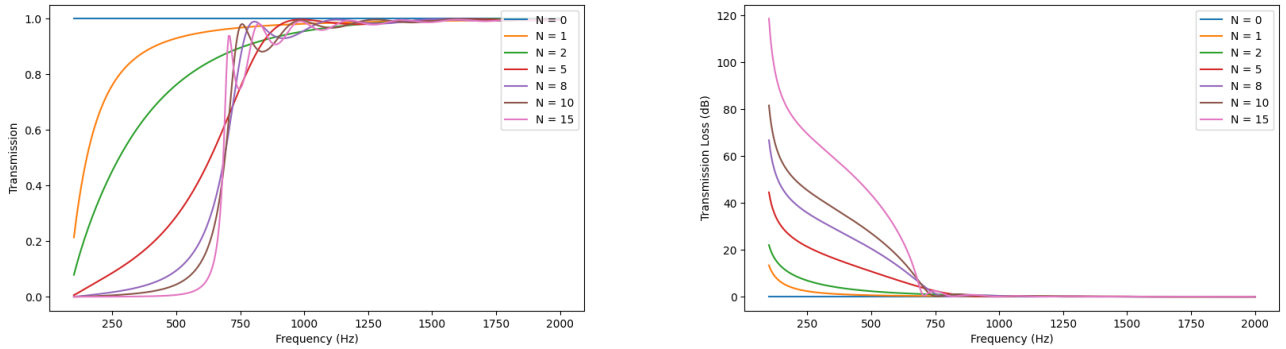

Figure 10: Frequency response for a water-air ($l_{rn} = l_{rc}$) filled system with different number of resonators.

to shift towards the lower frequency range. In addition, the resonance bandwidth increases significantly. Consequently, near zero transmission is seen in the frequency range of approximately 100 - 600 Hz. After this frequency range, the transmission coefficient increases quickly. This response is similar to the inhomogeneous response found in research done by Boyun Liu and Liang Yang [8].

What is important to notice is that in all cases, adding resonators seems to have a positive effect on the intensity of the peak. Alongside this, a slight increase in the attenuation bandwidth can be observed as well.

4.1.2 The effect of adding resonators

Using the cost function from Equation 19, the effect of adding multiple resonators was analysed. The frequency range used for the different systems was 100-1000 Hz, as this is the range that needs to be attenuated. Given previous observation, the homogeneous cases do not show attenuation in this range as their resonance frequency falls outside of this range. Therefore, only the inhomogeneous case will show considerable decrease in transmission as can be seen in Figure 11.The cost function for this system converges to around 0.3 transmission.

4.1.3 Optimizing l_{rn}/l_{rc}

To find the effect and optimum ratio for the resonator's neck and cavity, the cost function and the transmission coefficient were compared for N = 1, 2, 3, 5, 10 and 15. In Figure 31, the cost function

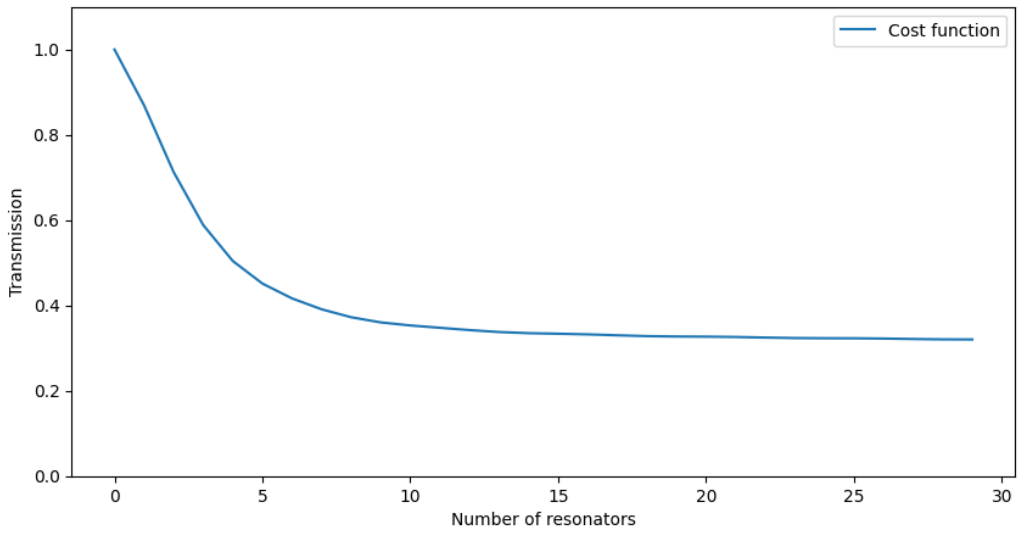

Figure 11: 1 resonator system with increasing r_w (m) for the inhomogeneous system.

and transmission coefficient for N = 5 can be seen. Because all figures showed the same optimal ratio, the other results can be found in Figure 28 in the Appendix.

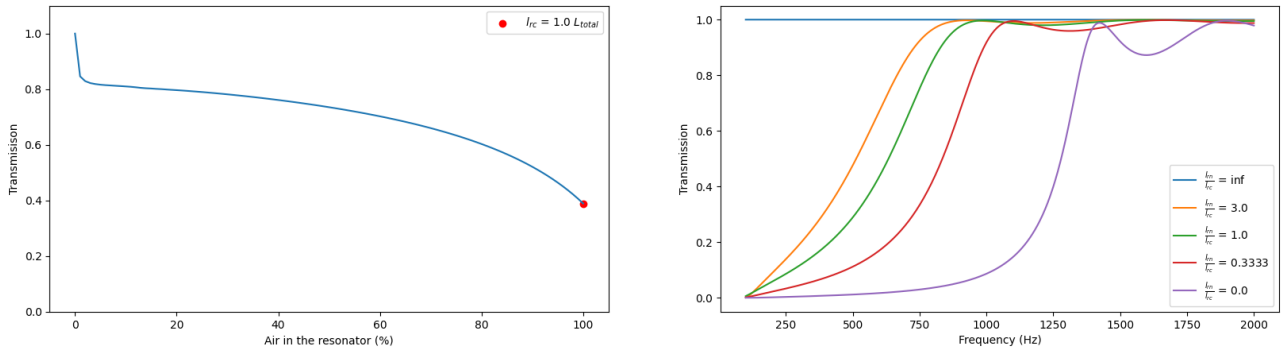

Figure 12: Cost function with increasing l_{rc} and the transmission coefficient for different water-air ratio's while N = 5.

From this figure, it is evident that in the inhomogeneous instance, the resonators perform most efficiently when their volume is filled solely with air as the operating medium. Considering it is extremely difficult, if not impossible, to acquire and maintain this ratio throughout operation, a more realistic figure of 90% is utilised in the remaining models.

4.1.4 Optimizing L_n

It can be seen from Figure 11 that the effect of adding more resonators has diminished considerably around 10 resonators. Therefore, modelling and optimisation was done for a 10 resonator system.

Using the three optimization methods, various configurations have been found. All these configurations were again assessed using the cost function. The results of these optimization methods can be found below in Table 1, where the subscripts f and b describe the forwards and backwards optimization methods. The most efficient configuration (3_b) was then dynamically solved again using the `scipy.optimize.minimize` module which resulted in the lowest average transmission (3_{sb}).

	$L_2(m)$	$L_3(m)$	$L_4(m)$	$L_5(m)$	$L_6(m)$	$L_7(m)$	$L_8(m)$	$L_9(m)$	$L_{10}(m)$	J
0	0.2	0.2	0.2	0.2	0.2	0.2	0.2	0.2	0.2	0.01733794511
1	0.0223	0.1790	0.0223	0.1007	0.0399	0.0732	0.0223	0.0223	0.0380	0.01485543612
2_f	0.0223	0.1790	0.1007	0.1183	1	0.2496	0.1575	0.1457	0.4416	0.01692701720
2_b	0.0223	0.1452	0.138	0.1733	0.0949	0.0773	0.0264	0.0264	0.0264	0.01649387237
3_f	0.0223	0.1790	0.1007	0.1183	1	0.2496	0.1575	0.1457	0.4416	0.01692701720
3_b	0.0223	0.1420	0.0768	0.0920	0.2885	0.1431	0.1455	0.1469	0.0645	0.00987555465
3_{sb}	0.02235	0.1248	0.1432	0.1405	0.1437	0.1405	0.1467	0.1472	0.0645	0.00799516348

Table 1: The periodic and all optimized configurations with 90% air in the resonator and their corresponding value for the cost function.

The frequency response that corresponds to the optimized system can be found below in Figure 13. The transmission in the frequency range has now decreased to a maximum of $\approx 4\%$. Therefore it can be said that the optimization of the water-air ratio and resonator placement resulted in lower transmission compared to Figure 11, which is in line with the desired outcome. The other frequency responses of the optimized systems can be found in the Appendix.

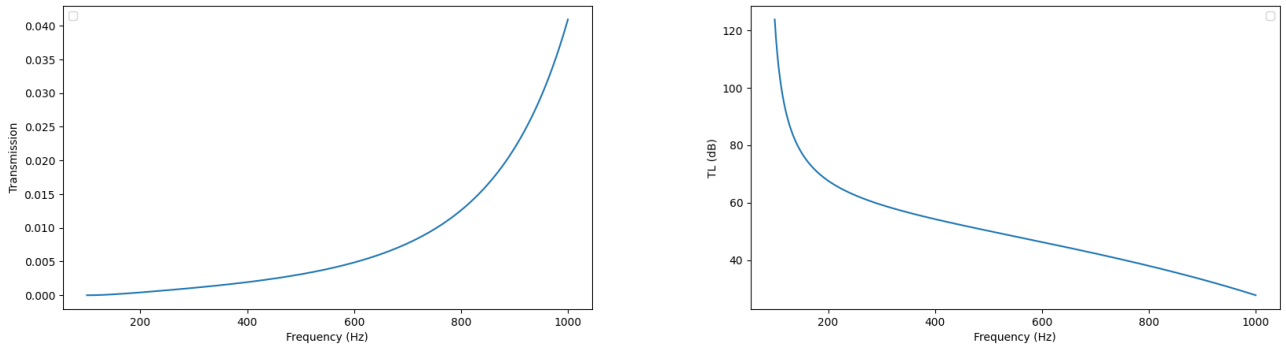

Figure 13: Transmission coefficient and TL for the best configuration obtained through optimization method 3 with 90% air in the resonator.

4.2 COMSOL results

To verify the analytical solutions, the periodic and final optimized arrangement were analysed using the FEM. The geometries and their corresponding mesh are presented in the figure below. It is essential to highlight that in the pressure distribution plots given in the following sections, the absolute value of the pressure is taken. This is done to more clearly illustrate what happens in and around the resonators.

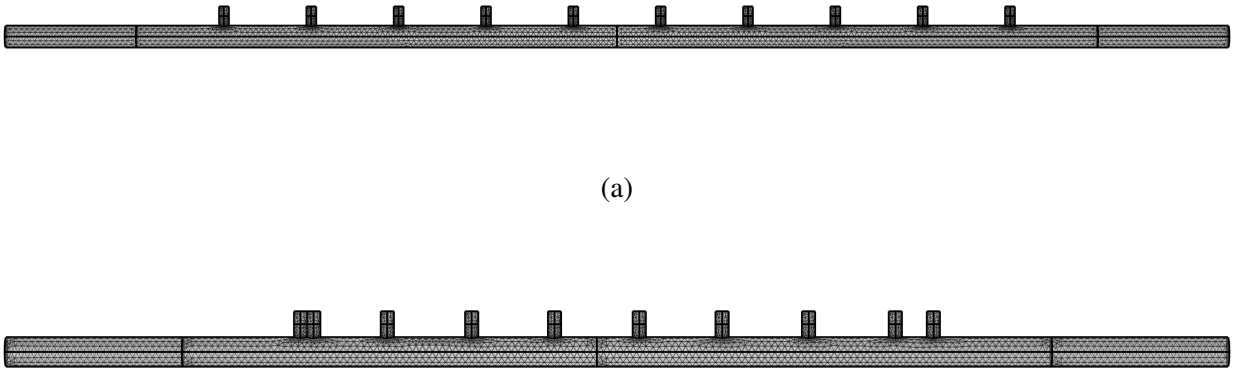

(a)

(b)

Figure 14: Geometry and mesh for the (a) periodic and (b) optimized configuration.

4.2.1 Waveguide

To clearly depict the effect of the sideloaded resonators, firstly the waveguide is analysed. The pressure distribution in the homogeneous air and water case can be found in Figure 20.

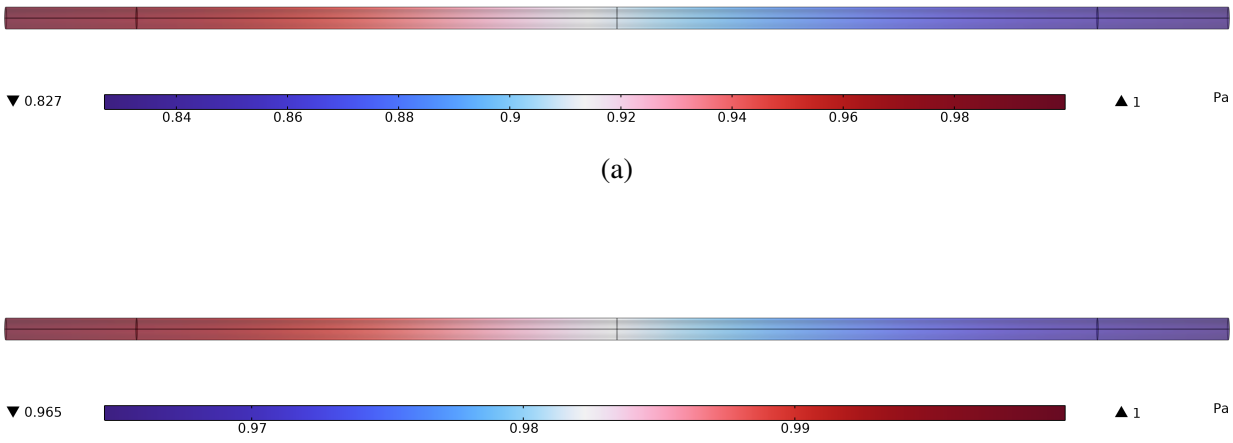

(a)

(b)

Figure 15: Pressure distribution for the (a) air and (b) water filled system.

As can be seen, most of the wave is transmitted with 17.3% and 3.5% of the pressure being absorbed through viscus effects in the air and water case respectively. This difference in attenuation can be attributed to the larger δ in air than in water.

4.3 Homogeneous

In this section, again the pressure distribution is given for the homogeneous air and water cases. This time however, all resonators are side loaded to the system. The following plots show the distribution during and out of resonance.

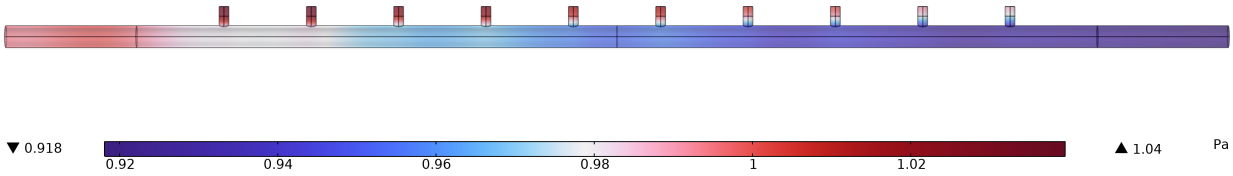

(a)

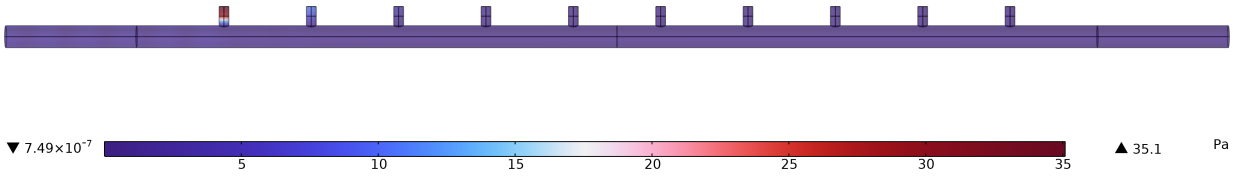

(b)

Figure 16: Pressure distribution for air (a) out of resonance (400 Hz) and (b) during resonance (1875 Hz).

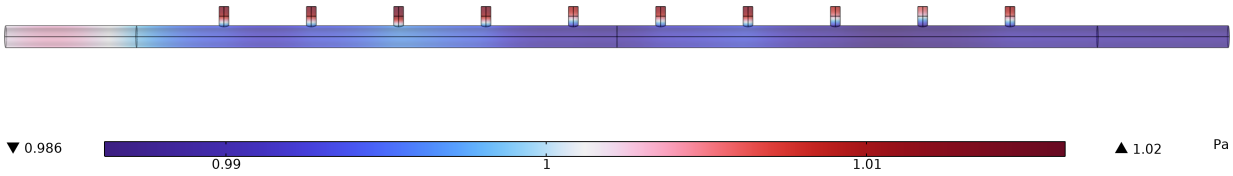

(a)

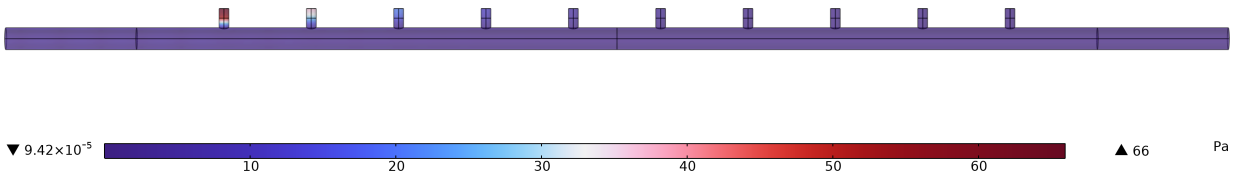

(b)

Figure 17: Pressure distribution for water (a) out of resonance (1000 Hz) and (b) during resonance (7950 Hz).

The plots in resonance show a much higher pressure in the resonators than the plots that are out of resonance. Also, the minimum pressure found in the geometry is more than four orders of magnitude

smaller. To see more clearly what happens at a single resonator during resonance, an isosurface plot can be seen below in Figure 18. This figure more clearly depicts the radiating and point like acoustic impact of the resonator. The transmission, reflection and absorption of both systems is presented in Figure 19.

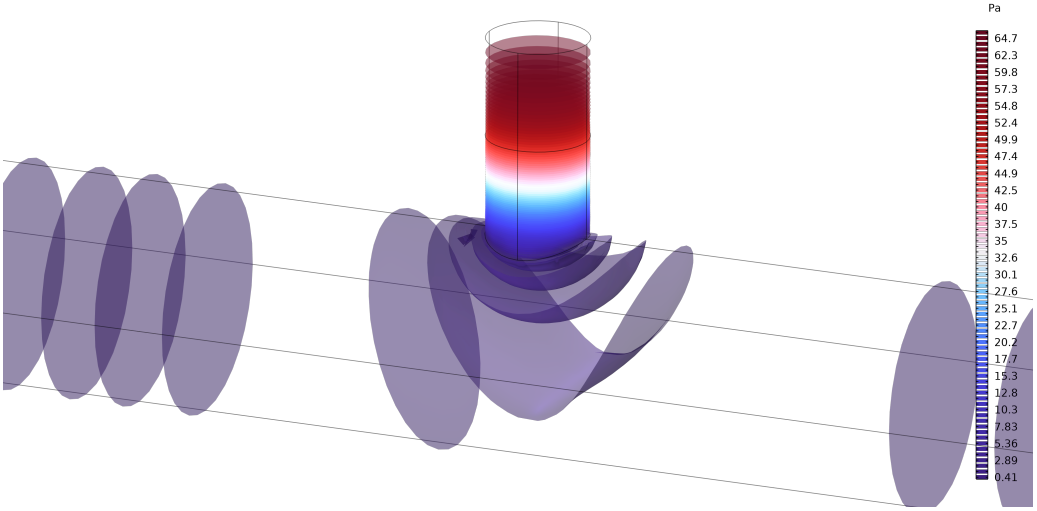

Figure 18: Isosurface pressure distribution plot for a homogeneous water system during resonance at 7950 Hz.

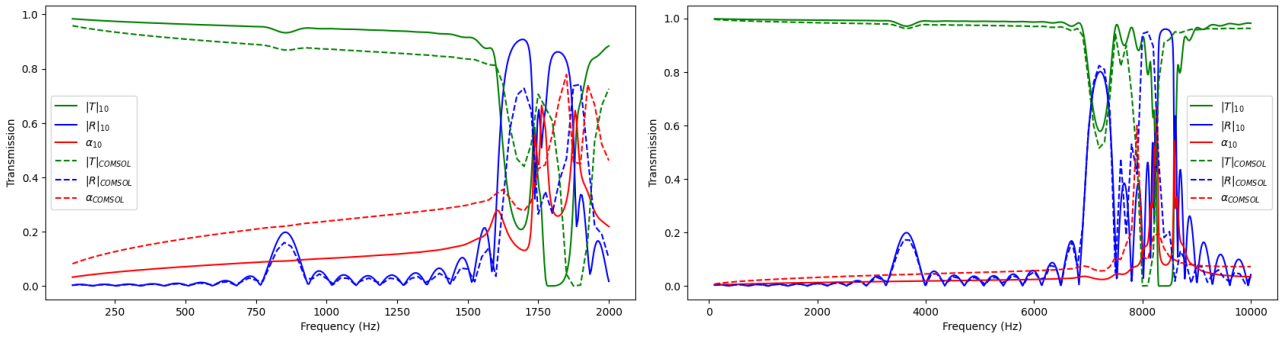

(a) (b)

Figure 19: The frequency response of the transmission, reflection and absorption coefficients in the homogeneous (a) air and (b) water system.

4.3.1 Inhomogeneous

For the inhomogeneous system, the pressure distribution plots are given for the periodic and optimized configuration.

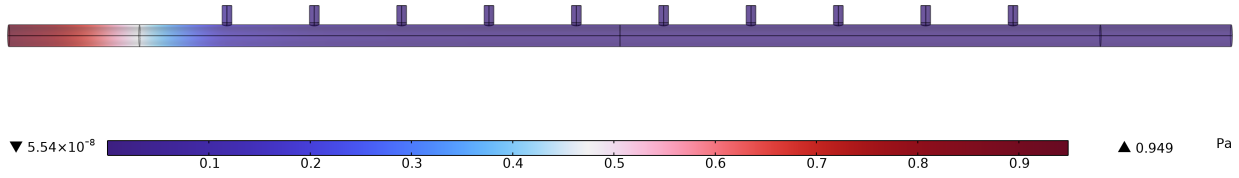

(a)

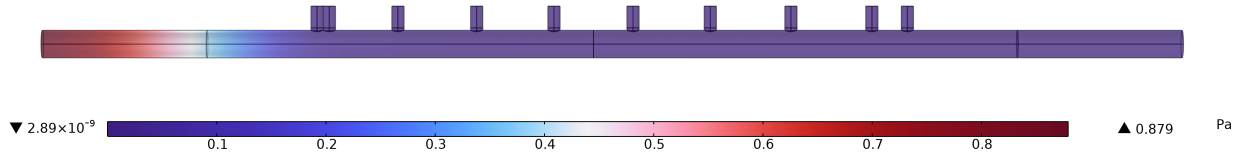

(b)

Figure 20: Pressure distribution for the (a) periodic and (b) optimized inhomogeneous system with 90% of the resonator filled with air at a frequency of 200 Hz.

From these plots, the difference in attenuation is less visible. It can however be noted that the minimum value is lower for the optimized configuration while its wave guide length is slightly shorter which allows for less viscous losses. To give more insight on what happens with different volumes of air in the resonator, another isosurface plot of the first resonator is given below.

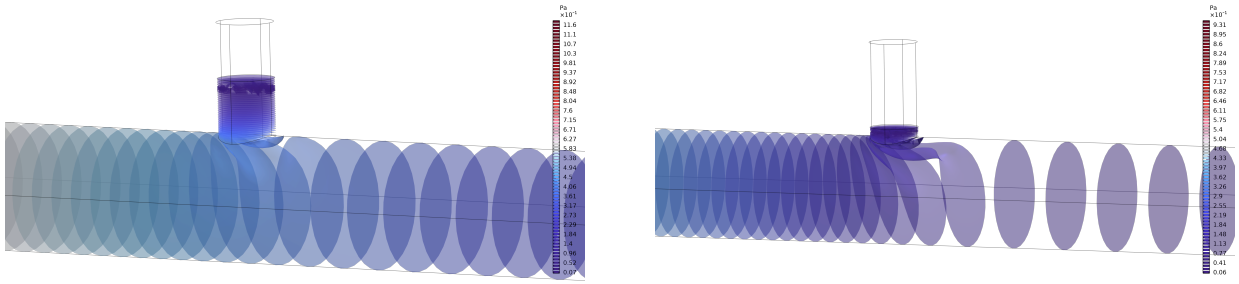

(a) (b)

Figure 21: Pressure distribution using isosurfaces for the first resonator which is (a) 50% and (b) 90% filled with air at a frequency of 200 Hz.

These isosurfaces more clearly visualise the increased attenuation at the resonators opening. The transmission, reflection and absorption coefficients of both the periodic and optimized configuration are shown in Figure 22. These plots also show the difference between having 50% or 90% air volume in the resonator, causing an increase in the attenuation bandwidth in both the analytical and FEM solutions.

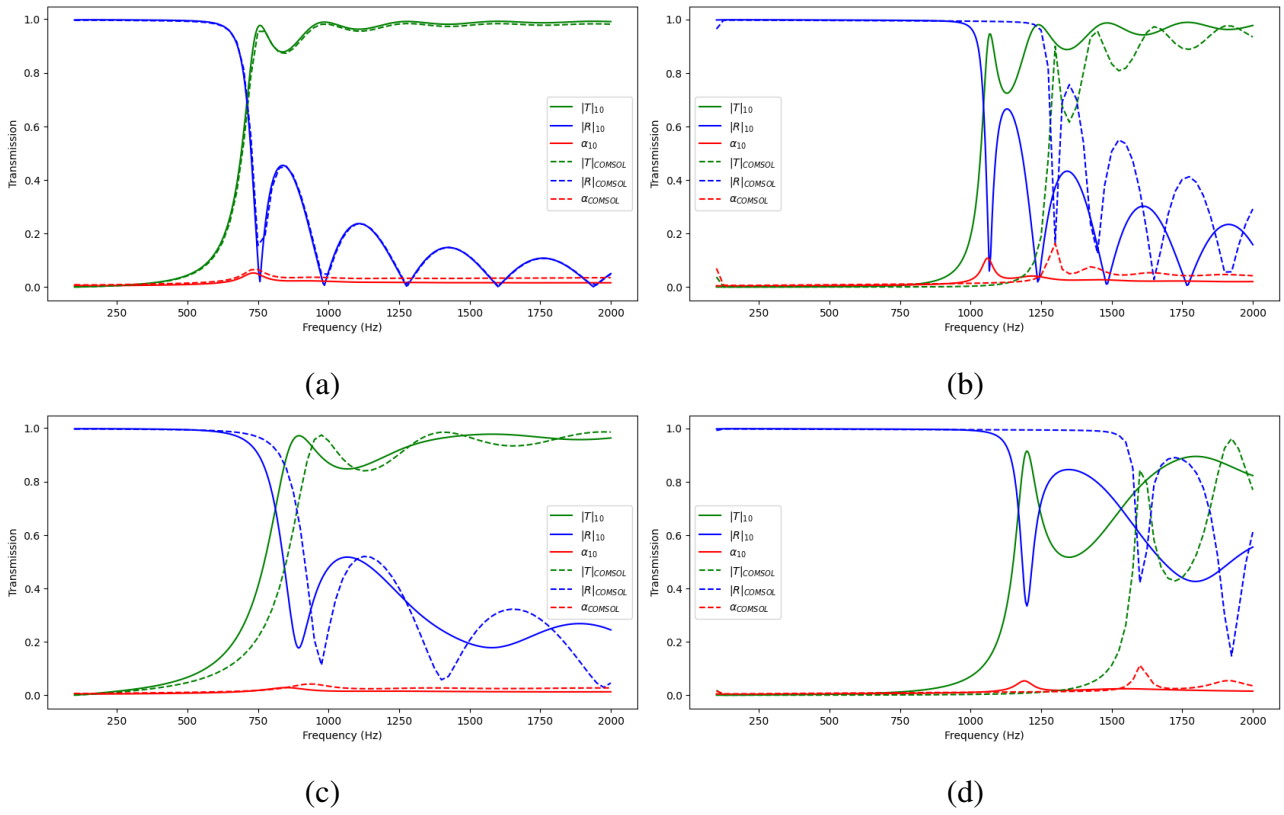

(a) (b)

(c) (d)

Figure 22: The transmission, reflection and absorption coefficients in the inhomogeneous system. (a) and (b) showcase the periodic geometry, while (c) and (d) demonstrate the optimized system. Additionally, (a) and (c) depict the results using a resonator that is for 50% filled with air, whereas (b) and (d) uses a 90% air-filled resonator.

The COMSOL and analytical results show very similar responses in the 50% air-filled resonator system. This similarity however weakens when the water-air ratio in the resonator is altered. To investigate the cause of this, various variables in the analytical solutions were altered one by one. In the figure below, the length correction (Δl) was manually tuned to comes as close to the COMSOL solution as possible. This newly found length correction is depicted as Δl_t.

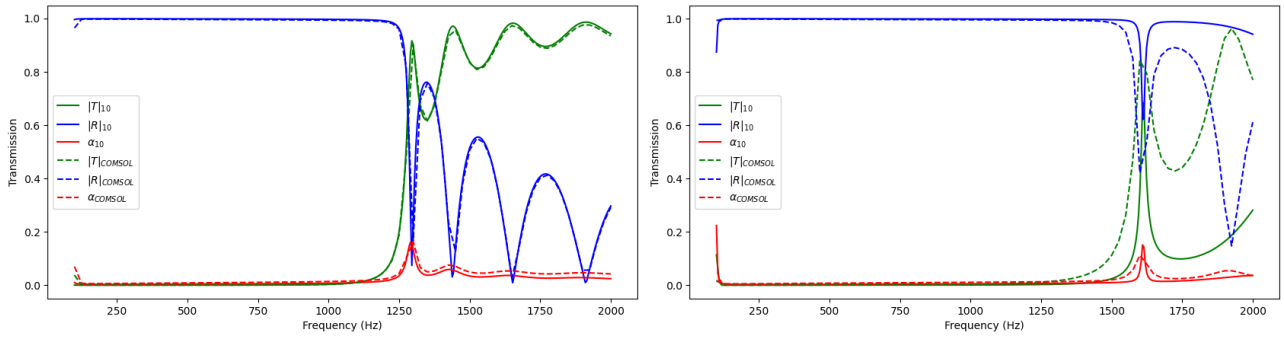

(a) (b)

Figure 23: The transmission, reflection and absorption coefficient for the (a) periodic ($\Delta l_t = 0.42\Delta l$) and (b) optimized system ($\Delta l_t = 0.1\Delta l$).

To investigate the behaviour of Δl_t, multiple water-air mixtures were plotted using the periodic configuration. These plots can be found in the Appendix. Plotting Δl_t in terms of Δl against the percentage of air in the resonator resulted in a plot having a close to linear relation. This result is depicted in the figure below.

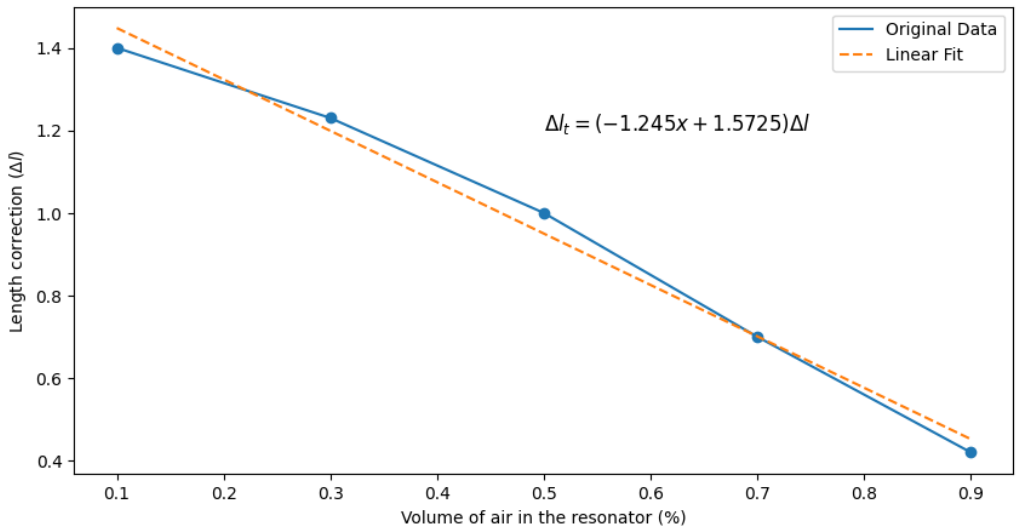

Figure 24: Air volume (%) versus Δl_t given in terms of Δl. x represents the volume of air in the resonator in percentage.

This technique could not be applied to the optimized configuration as changing the length correction alone did still leave a considerable difference between the two results.

5 Discussion

This thesis aimed to investigate the transmitting behaviour of a waveguide sideloaded with identical cylinderical resonators for a homogeneous and inhomogeneous system. Consequently, determining the optimum separation distances between the resonators and their optimum water-air ratio in the inhomogeneous case. Using analytical models that utilizes the TMM, cost function and a second model constructed through COMSOL, various results have been obtained. The quality and accuracy of these results will be discussed in this section.

5.1 Homogeneous vs. Inhomogeneous Systems

To better understand the effect of filling the resonators with air, two homogeneous cases were modelled next to the inhomogeneous case. The first homogeneous system was filled with air and the second system was filled with water. The frequency responses of these systems were as expected, with both resonance frequencies positioned around their theoretical value, causing a short decrease in transmission. When resonators were added, the response became increasingly irregular and another decrease in transmission occurred before the resonance frequency. These irregularities can be associated with the increasing complexity of the final transfer matrix **T** when more resonators are added to the TMM, therefore causing additional attenuation before the resonant peak. To ensure that these irregularities were not mathematical errors, they were investigated using the FEM. In Figure 19, it is observed that both results show similar behaviour. The fluctuations can therefore be attributed to additional scattering caused by the resonators. The biggest difference between the two solutions can be seen for air. In this instance, the FEM yielded higher attenuation through viscous effects and lower attenuation during resonance.

For the inhomogeneous system, the greatest difference in the analytical calculations lays in the transfer matrix of the resonant element. In this segment of the computations, the neck and cavity are assigned different material properties, hence, each having a different wavenumber and impedance. This causes terms that would otherwise be cancelled out in Equation 16, to be taken into account. This term is dependent on the impedance match of the two fluids, causing the result to highly differ. To give a clearer insight to the different behaviour of the ratio Z_{rn}/Z_{rc} in the homogeneous and inhomogeneous case, its frequency response is included in Figure 25 in the Appendix. This response consequently influences Equation 21, where the impedance ratio between the resonator and the waveguide is crucial in determining the transmission. When $Z_w >> Z_r$, minimum transmission occurs. Although a different response was expected for the inhomogeneous system, the results were still surprising. It was expected that the addition of air in the resonator would lower the resonance frequency. However, the fact that it would accomplish this so effectively and for such a greater bandwidth than the homogeneous cases was not anticipated. The FEM solutions validated this response.

Although many differences in the frequency responses of the homogeneous and inhomogenous systems were observed, an important similarity was apparent. The similarity being the increase in TL for every added resonator, proving the increase of resonators to be essential for higher attenuation. This result was highlighted in Section 4.1.1. Considering that the optimization was specifically focused on the frequency range from 100-1000 Hz, the inhomogeneous system appeared to be a highly more efficient approach for sound mitigation. Therefore, answering the question governing the efficiency of homogeneously filled resonators during low-frequency attenuation.

5.2 Optimization inhomogeneous system

Firstly, the optimum water-air ratio was obtained so it could be applied in the next optimization processes. This was done using the cost function. The effect of the water-air ratio was analysed for systems with 1, 2, 3, 5, 10 and 15 resonators, all showing similar results. It could therefore be concluded using the analytical model, that increasing the volume of air in the resonator positively influences attenuation. This result was also confirmed using FEM and displayed in Figure 22. The reasoning behind this improved attenuation can be traced back to Equation 16 as well. Now it is not the impedance ratio Z_{rn}/Z_{rc} and wavenumbers that plays an important role as this is not dependent on the volume, but the lengths l_{rn} and l_{rc}. The effect of increasing l_{rc} was also investigated using the FEM. Using isosurfaces, the increased acoustic impact was clearly visualised and in Figure 22, an even greater increase in the attenuation bandwidth for greater air volumes than the analytical solutions could be observed. The difference between these results was investigated and concluded to be in the length correction (Δl) of the resonator. The relation between the tuned length correction Δl_t and the air volume percentage (x) was found to be Δl_t = (-1.245x + 1.5725)Δl. However, because the tuning parameter was determined visually and only five different ratios were tested, this result is deficient in its accuracy.

Regarding the optimization of L_n, three different approaches were applied. All of these approaches utilizing the cost function. Initially, the cost function of the first optimisation technique was lower than that of the identical configurations found using optimisation methods 2 and 3_f, which was not as expected. Optimization method 3_b did, nonetheless, present an enhanced arrangement. This was again optimized to result in the most efficient configuration 3_{sb} with an average transmission of $\approx$ 0.8%. From Table 1, it can be seen that this value is less than half of the periodic arrangement. Therefore, the optimized arrangement proves to be a more effective approach.

If more iterations were done using the third optimization method, it is likely that a lower transmission could have been obtained. Nonetheless, the average transmission is sufficiently low to produce the necessary level of attenuation in sound. It can therefore be said that this optimization process was successful. With the optimum values for $L_{2\rightarrow10}$ found to be 0.02235 m, 0.1248 m, 0.1432 m, 0.1405 m, 0.1437 m, 0.1405 m, 0.1467 m, 0.1472 m and 0.0645 m respectively. Using the model in COMSOL, this configuration was also found to have an increased attenuation. The analytical and FEM solutions for the optimized configuration did however show a lower correlation in their responses. This dissimilarity increased when the air volume in the resonator was set to increased. The analytical and FEM solutions do however show increased attenuation in the optimized configuration.

Lastly, because in all optimization the cost function was applied, its quality needs to be assessed. Although this function is efficient in calculating the average transmission, it does not include clear insight to any dips or peaks in the frequency response. As a result, high intensities could possible still pass through some of the systems that were analysed. Examples of this are the optimized configurations 2_f and 3_f found in the Appendix. This issue fortunately, disappears when the corresponding TL or transmission coefficient are plotted and examined visually. Therefore, this is not regarded as problematic and the quality of the optimization technique is validated.

5.3 Future research

To return to the motivation for this research, the findings can be translated back to the resonant AMM shown in the Introduction. Where the distances L_n are the distances between the resonators on the AMM panel and r_w the vertical separation of the system. Furthermore, the differences between homogeneous and inhomogeneous resonators together with the findings on the optimum water-air ratio can be used to determine if the resonators should be refilled during operation.

If this model was to be further investigated, the transmitting behaviour could be tested with a plane wave entering the waveguide at an oblique angle. Additionally, the radius of the cavity could be increased to observe the dissimilarity between utilizing a quarter-wave tube or a Helmholtz resonator. Furthermore, to improve the understanding of inhomogeneously filled resonators, further research could be conducted on the accurate representation of the length correction (Δl), as problems arose between the FEM and analytical solution in this research. Lastly, the differences in the FEM and analytical solutions for the optimized arrangement require further clarification.

6 Conclusion

This thesis researched the acoustic transmitting behaviour of a waveguide sideloaded with cylindrical resonators. This was done for two homogeneous cases using air or water and one inhomogeneous case where the waveguide was filled with water and the resonator with water and air. It was found that increasing the amount of resonators in all systems positively influenced the total attenuation. In addition, the inhomogeneous system resulted in having a lower and wider frequency bandwidth where attenuation could take place. Therefore, the inhomogeneous system displayed greater efficiency than expected. The water-air ratio in the resonator was determined to show maximum attenuation when only air occupied the resonators volume. Altering this ratio did however cause diminished similarity in the analytical and FEM results. This difference was attributed to an inaccurate representation of the length correction in the periodic configuration. The outcome of the resonator separation length optimization was successful, with the cost function having a value of approximately 0.08% which was less than half the value of the periodic configuration. The optimized distances ($L_{2\rightarrow 10}$) were found to be 0.02235 m, 0.1248 m, 0.1432 m, 0.1405 m, 0.1437 m, 0.1405 m, 0.1467 m, 0.1472 m and 0.0645 m respectively.

To improve the understanding of inhomogeneously filled resonators, additional research can be conducted researching a correct representation of the length correction. Furthermore, the differences between the FEM and analytical solutions in the optimized configuration could be researched.

Bibliography

[1] B. Sztyler and P. Strumiłło *Archives of Acoustics*, vol. vol. 47, no. No 1, pp. 3–14, 2022.

[2] Y. Chen, "Acoustical transmission line model for ultrasonic transducers for wide-bandwidth application," *Acta Mechanica Solida Sinica*, vol. 23, no. 2, pp. 124–134, 2010.

[3] D. M. Bellmann, A. May, D. T. Wendt, S. Gerlach, P. Remmers, and J. Brinkman, "Technical report underwater noise during percussive pile driving ... - itap," May 2020. url=https://www.itap.de/media/experience_report_underwater_era-report.pdf.

[4] E. C. Energy, "Offshore renewable energy," 2022. url=https://energy.ec.europa.eu/topics/renewable-energy/offshore-renewable-energy_en.

[5] K. M. Lee, A. R. McNeese, P. S. Wilson, and M. S. Wochner, "Using arrays of air-filled resonators to reduce underwater man-made noise," Aug 2023.

[6] A. Technologies, "Sound. science.," 2022. url=https://adbmtech.com/.

[7] S. Rienstra and A. Hirschberg, *An introduction to acoustics*. Technische Universiteit Eindhoven, 2004. Extended and revised edition of IWDE 92-06.

[8] B. Liu and L. Yang, "Transmission of low-frequency acoustic waves in seawater piping systems with periodical and adjustable helmholtz resonator," *Journal of Marine Science and Engineering*, vol. 5, no. 4, 2017.

[9] *Acoustic Impedance at Normal Incidence of Fluids. Substitution of a Fluid Layer for a Porous Layer*, ch. 2, pp. 15–27. John Wiley Sons, Ltd, 2009.

[10] F. N. Amjad, "Sound attenuation - university of cambridge." https://www.phase-trans.msm.cam.ac.uk/2000/amjad/b.pdf. Accessed: 2024-02-21.

[11] Caltech, "Lecture 14 - 6 reflection and transmission," Dec 2019. url=https://www.its.caltech.edu/~xcchen/img/Ph12a2019/lecture_notes/lecture1114.pdf.

[12] M. Schwartz, "Lecture 9: Reflection, transmission and impedance." url=https://scholar.harvard.edu/files/schwartz/files/lecture9-impedance.pdf.

[13] C. Zwikker and C. W. Kosten, *Sound absorbing materials / by C. Zwikker and C.W. Kosten*. New York: Elsevier Pub. Co., 1949.

[14] E. Britannica, "The helmholtz resonator." https://www.britannica.com/science/sound-physics/The-Helmholtz-resonator. Accessed: 2024-02-19.

[15] S. He and D. W. Herrin. PhD thesis, Master of Science in Mechanical Engineering (MSME), 2017.

[16] P. K. Kundu, I. M. Cohen, and D. R. Dowling, *Fluid mechanics*, vol. 6. Academic Press, 2016.

[17] O. Richoux and V. Pagneux, "Acoustic characterization of the hofstadter butterfly with resonant scatterers," *Europhysics Letters*, vol. 59, p. 34, jul 2002.

[18] G. Theocharis, O. Richoux, V. R. García, A. Merkel, and V. Tournat, "Limits of slow sound propagation and transparency in lossy, locally resonant periodic structures," *New Journal of Physics*, vol. 16, p. 093017, sep 2014.

[19] "Transfer matrix." http://assets.press.princeton.edu/chapters/s8695.pdf. Accessed: 2024-02-02.

[20] A. Dell, A. Krynkin, and K. Horoshenkov, "The use of the transfer matrix method to predict the effective fluid properties of acoustical systems," *Applied Acoustics*, vol. 182, p. 108259, 2021.

[21] COMSOL Application Gallery, "Helmholtz resonator with porous layer." https://www.comsol.com/model/helmholtz-resonator-with-porous-layer-96871. Accessed: 2024-02-20.

[22] "Port." https://doc.comsol.com/6.2/doc/com.comsol.help.aco/aco_ug_pressure.05.027.html. Accessed: 2024-02-23.

Appendices

A Analytical solutions

A.1 Z_{rn}/Z_{rc} frequency response.

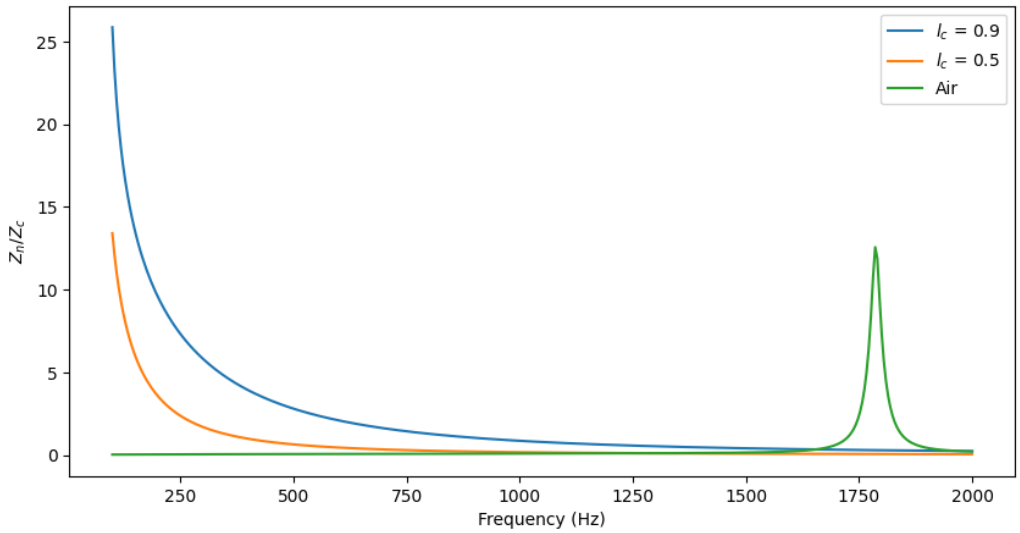

Figure 25: The frequency response of Z_{rn}/Z_{rc} for the inhogeneous case ($l_c = 0.9, l_c = 0.5$) and the homogeneous air case.

A.2 Waveguide radius determination

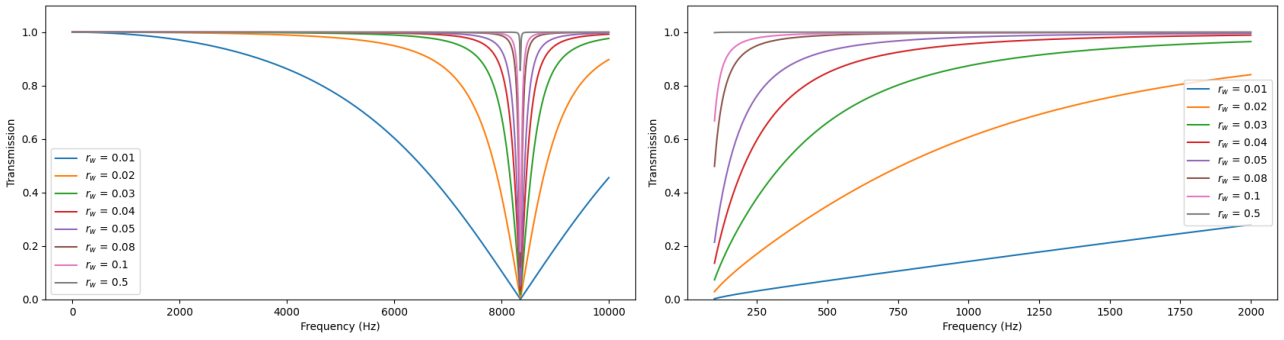

(a) (b)

Figure 26: 1 resonator system with increasing r_w (m) for an (a) water and (b) water-air filled system.

A.3 Optimizing l_{rn}/l_{rc}

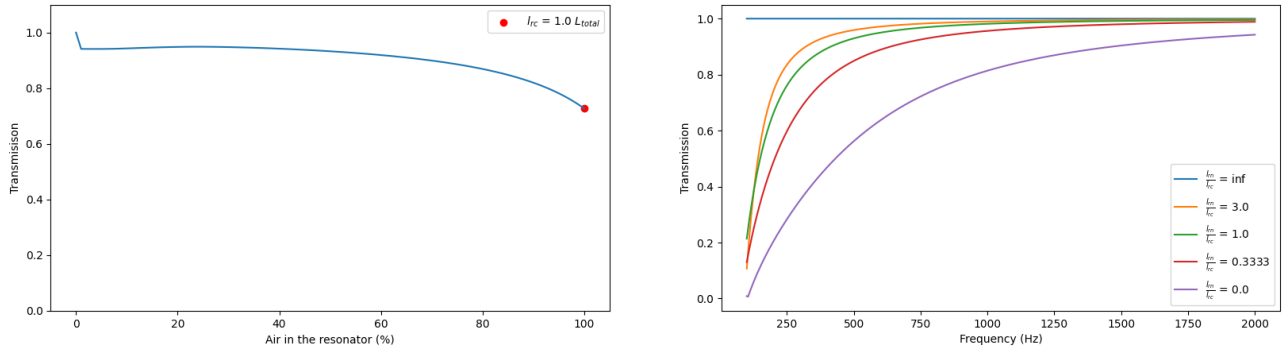

(a)

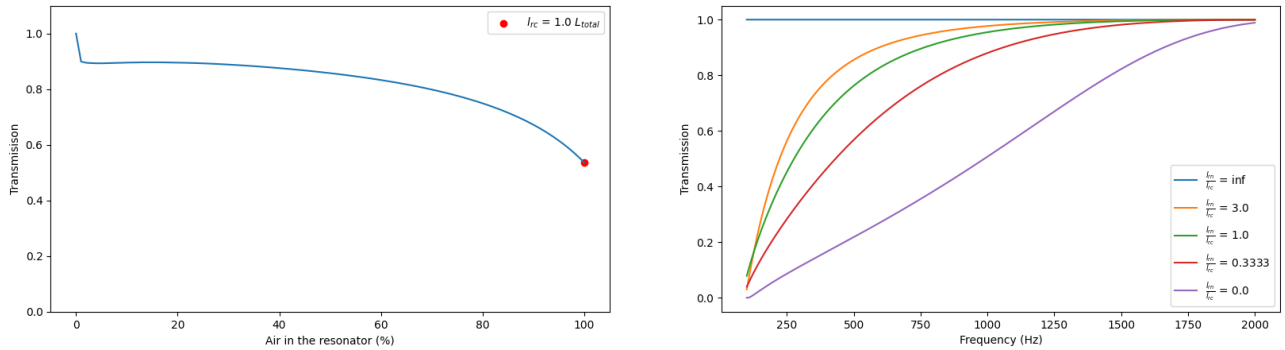

(b)

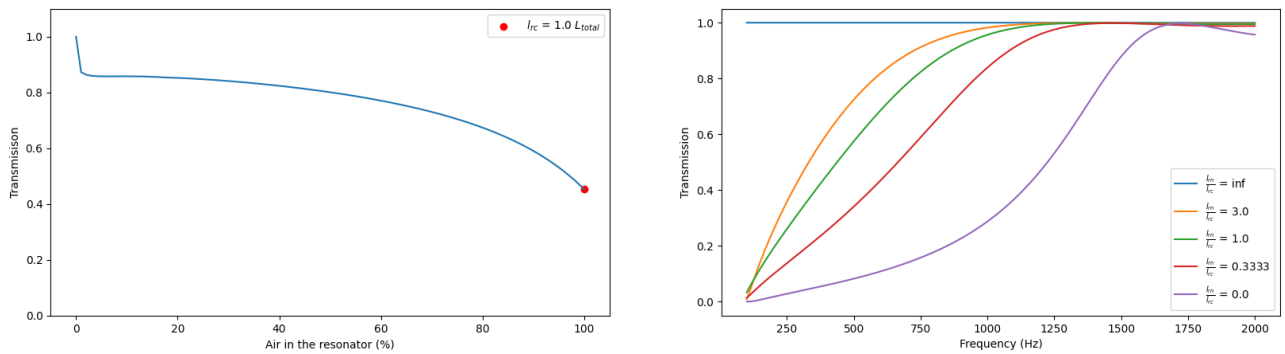

(c)

Figure 27: Water-air ratio optimization for (a) N = 1, (b) N = 2, (c) N = 3, (d) N = 10 and (e) N = 15.

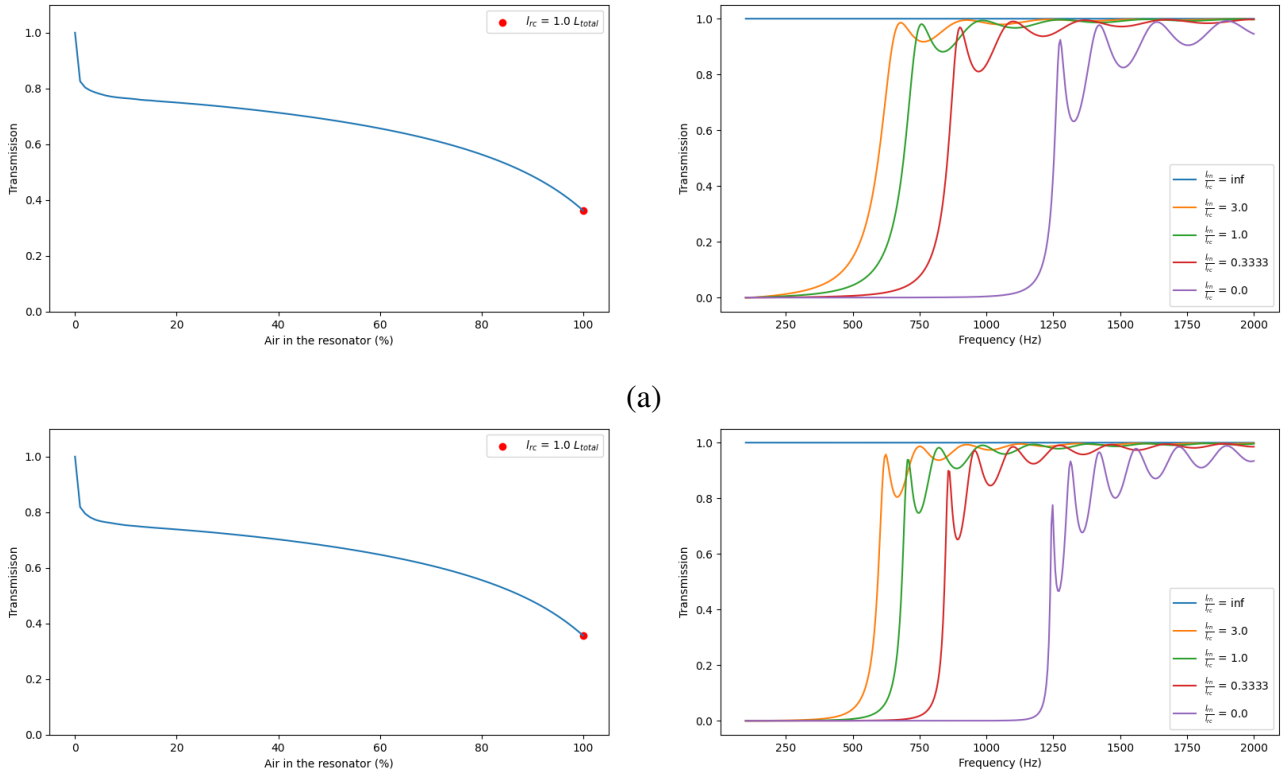

(a)

(b)

Figure 28: Water-air ratio optimization for (a) N = 10 and (b) N = 15.

A.4 Optimization methods for L_n

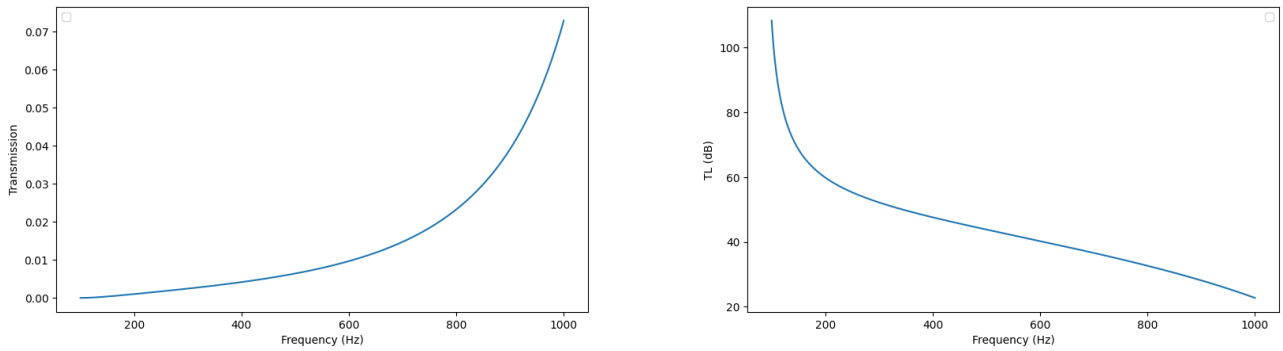

Figure 29: Optimization method 1 frequency response

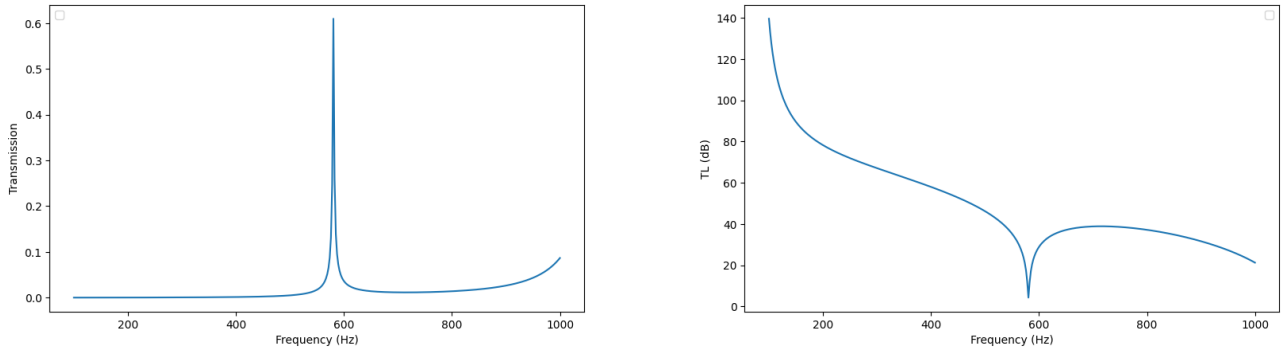

Figure 30: Optimization method 2_f and 3_f frequency response

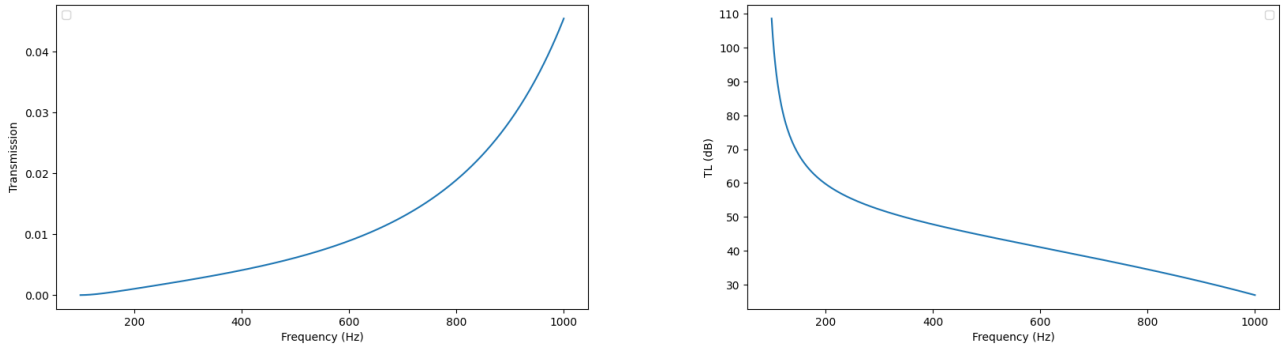

Figure 31: Optimization method 2_b frequency response.

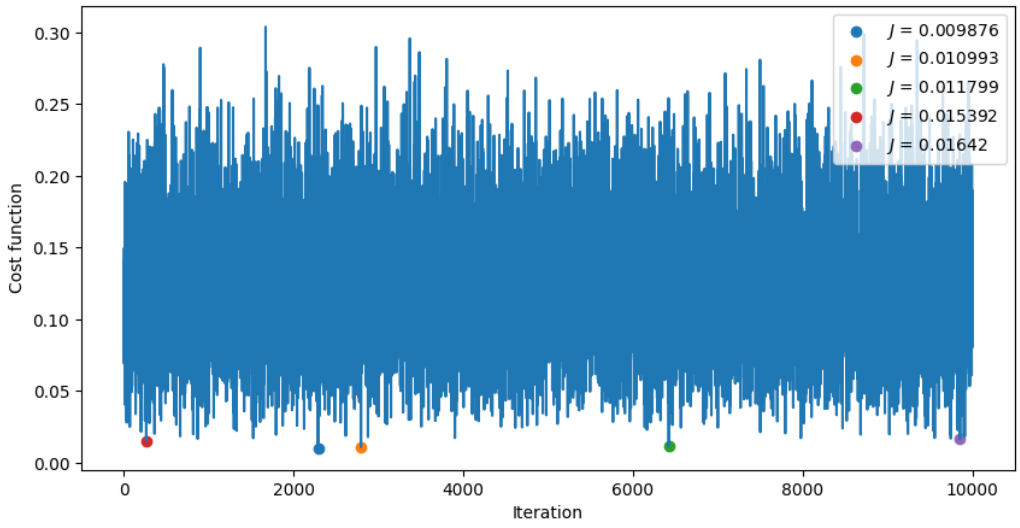

Figure 32: Random L_n configurations their cost functions for N = 5.

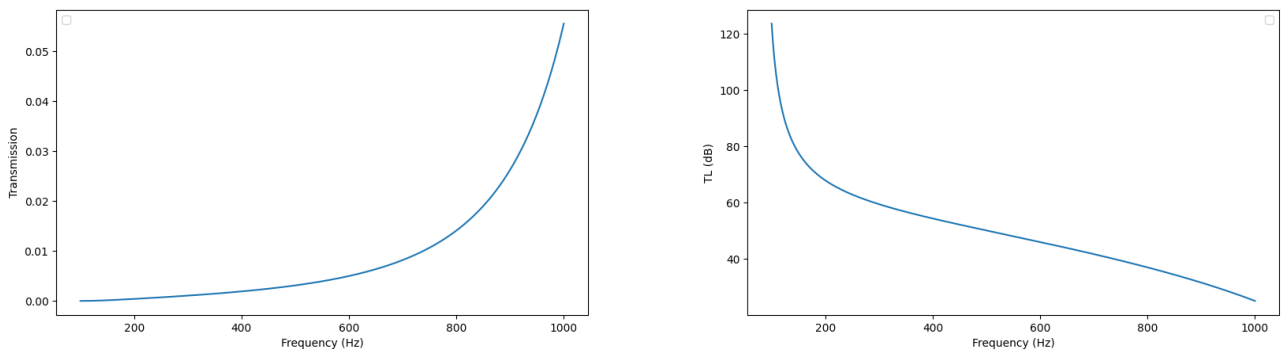

Figure 33: Optimization 3_b method frequency response.

B Code for the analytical solutions

```
import matplotlib.pyplot as plt
import numpy as np

#Transmission function used
def transmittance(f, resonators, distance1andN, distance2, distance3, distance4,
    distance5, distance6=0, distance7=0, distance8=0, distance9=0, distance10=0,
    Radius_tube=0.05, medium=2):

  #frequency dependent formulas and constants
  d = distance1andN
  w = distance2
  x = distance3
  y = distance4
  q = distance5
  a = distance6
  b = distance7
  m = distance8
  g = distance9
  h = distance10

  #frequency dependent formulas and constants
  omega = 2 * np.pi * f

  R = Radius_tube
  r = 0.011176
  Area = np.pi * R**2
  area = np.pi * r**2

  rat = r/R
  #Length correction
  l_cor = 0.82*(1 - 0.235*rat - 1.32*rat**2 + 1.54*rat**3 - 0.86*rat**4)*r

  #Material properties
  #AIR
  c = 343  #sound speed
  Pr = 0.71   #pradntl
  gamma = 1.4    #heat capacity
  rho = 1.293       #density
  mu = 1.839 * 10**-5       #Viscocity
  delta = np.sqrt((2*mu)/(rho*omega))     #Viscous boundary layer thickness
  delta_r = np.sqrt((2*mu)/(rho*omega))

  #water
  c_w = 1461
  Pr_w = 7
  gamma_w = 1.330
  rho_w = 998
  mu_w = 1.0016 * 10**-3
  delta_w = np.sqrt((2*mu_w)/(rho_w*omega))
  delta_wr = np.sqrt((2*mu_w)/(rho_w*omega))


  #Constants for the impedance and wavenumber
  beta = (1 - 1j) / np.sqrt(2)
  chi = np.sqrt(Pr)
```

```
54  chi_w = np.sqrt(Pr_w)
55
56  #Air
57  if medium == 0:
58    #Waveguide
59      k_v = (omega / c) * (1 + ((beta * delta) / R) * (1 + (gamma - 1) * chi))
60      Z_v = ((rho * c)/Area)  * (1 + ((beta * delta) / R) * (1 - (gamma - 1) *
    chi))
61
62    #Resonator
63      k = (omega / c) * (1 + ((beta * delta_r) / r) * (1 + (gamma - 1) * chi))
64      Z = ((rho * c)/area) * (1 + ((beta * delta_r) / r) * (1 - (gamma - 1) *
    chi))
65
66      numerator = np.cos(k*l_n)*np.cos(k*l_c) - (Z / Z)*k*l_cor*np.cos(k*l_n)*np
    .sin(k*l_c) - (Z / Z)*np.sin(k*l_n)*np.sin(k*l_c)
67      denominator = (1 / Z)*np.cos(k*l_c)*np.sin(k*l_n) - (1 / Z)*l_cor*k*np.sin
    (k*l_n)*np.sin(k*l_c) + (1 / Z)*np.cos(k*l_n)*np.sin(k*l_c)
68
69      #Resonator impedance
70      Z_q = -1j * (numerator / denominator)
71
72  #Water
73  elif medium == 1:
74
75   #Waveguide
76      k_v = (omega / c_w) * (1 + ((beta * delta_w) / R) * (1 + (gamma_w - 1) *
    chi_w))
77      Z_v = ((rho_w * c_w)/Area)  * (1 + ((beta * delta_w) / R) * (1 - (gamma_w
    - 1) * chi_w))
78
79  #Resonator
80      k = (omega / c_w) * (1 + ((beta * delta_wr) / r) * (1 + (gamma_w - 1) *
    chi_w))
81      Z = ((rho_w * c_w)/area)* (1 + ((beta * delta_wr) / r) * (1 - (gamma_w -
    1) * chi_w))
82
83      numerator = np.cos(k*l_n)*np.cos(k*l_c) - (Z / Z)*k*l_cor*np.cos(k*l_n)*np
    .sin(k*l_c) - (Z / Z)*np.sin(k*l_n)*np.sin(k*l_c)
84      denominator = (1 / Z)*np.cos(k*l_c)*np.sin(k*l_n) - (1 / Z)*l_cor*k*np.sin
    (k*l_n)*np.sin(k*l_c) + (1 / Z)*np.cos(k*l_n)*np.sin(k*l_c)
85
86      Z_q = -1j * (numerator / denominator)
87
88  #Inhomogeneous
89  else:
90
91 #Waveguide
92      k_v = (omega / c_w) * (1 + ((beta * delta_w) / R) * (1 + (gamma_w - 1) *
    chi_w))
93      Z_v = ((rho_w * c_w)/Area)   * (1 + ((beta * delta_w) / R) * (1 - (gamma_w
     - 1) * chi_w))
94
95  #Resonator
96      #Water/air
97      Z_n = ((rho_w * c_w)/area) * (1 + ((beta * delta_wr) / r) * (1 - (gamma_w
    - 1) * chi_w))
```

```
98        k_n = (omega / c_w) * (1 + ((beta * delta_wr) / r) * (1 + (gamma_w - 1) *
    chi_w))
99        Z_c = ((rho * c)/area) * (1 + ((beta * delta_r) / r) * (1 - (gamma - 1) *
    chi))
100       k_c = (omega / c) * (1 + ((beta * delta_r) / r) * (1 + (gamma - 1) * chi))
101
102       numerator = np.cos(k_n*l_n)*np.cos(k_c*l_c) - (Z_n / Z_c)*k_n*l_cor*np.cos
    (k_n*l_n)*np.sin(k_c*l_c) - (Z_n / Z_c)*np.sin(k_n*l_n)*np.sin(k_c*l_c)
103       denominator = (1 / Z_n)*np.sin(k_n*l_n)*np.cos(k_c*l_c) - (1 / Z_c)*k_n*
    l_cor*np.sin(k_n*l_n)*np.sin(k_c*l_c) + (1 / Z_c)*np.cos(k_n*l_n)*np.sin(k_c*
    l_c)
104
105       #Resonator impedance
106       Z_q = -1j * (numerator / denominator)
107
108   #Possible extra length for the first and last L_n
109   Lextra = 0
110
111   din = d + Lextra
112   dout = d + Lextra
113   Tin = np.array([[np.cos(k_v * din), 1j * Z_v * np.sin(k_v * din)], [(1j / Z_v)
        * np.sin(k_v * din), np.cos(k_v * din)]]) #T1
114   Tout = np.array([[np.cos(k_v * dout), 1j * Z_v * np.sin(k_v * dout)], [(1j /
     Z_v) * np.sin(k_v * dout), np.cos(k_v * dout)]]) #T11
115
116   #Allowing for different lengths of T1
117   T1_1 = np.array([[np.cos(k_v * w), 1j * Z_v * np.sin(k_v * w)], [(1j / Z_v) *
     np.sin(k_v * w), np.cos(k_v * w)]])  #T2
118   T1_2 = np.array([[np.cos(k_v * x), 1j * Z_v * np.sin(k_v * x)], [(1j / Z_v) *
     np.sin(k_v * x), np.cos(k_v * x)]])  #T3
119   T1_3 = np.array([[np.cos(k_v * y), 1j * Z_v * np.sin(k_v * y)], [(1j / Z_v) *
     np.sin(k_v * y), np.cos(k_v * y)]])  #T4
120   T1_4 = np.array([[np.cos(k_v * q), 1j * Z_v * np.sin(k_v * q)], [(1j / Z_v) *
     np.sin(k_v * q), np.cos(k_v * q)]])  #T5
121   T1_5 = np.array([[np.cos(k_v * a), 1j * Z_v * np.sin(k_v * a)], [(1j / Z_v) *
     np.sin(k_v * a), np.cos(k_v * a)]])  #T6
122   T1_6 = np.array([[np.cos(k_v * b), 1j * Z_v * np.sin(k_v * b)], [(1j / Z_v) *
     np.sin(k_v * b), np.cos(k_v * b)]])  #T7
123   T1_7 = np.array([[np.cos(k_v * m), 1j * Z_v * np.sin(k_v * m)], [(1j / Z_v) *
     np.sin(k_v * m), np.cos(k_v * m)]])  #T8
124   T1_8 = np.array([[np.cos(k_v * g), 1j * Z_v * np.sin(k_v * g)], [(1j / Z_v) *
     np.sin(k_v * g), np.cos(k_v * g)]])  #T9
125   T1_9 = np.array([[np.cos(k_v * h), 1j * Z_v * np.sin(k_v * h)], [(1j / Z_v) *
     np.sin(k_v * h), np.cos(k_v * h)]])  #T10
126
127   T2 =  np.array([[1, 0], [(1 / Z_q), 1]])  #Resonator
128
129 #Resonators 0 - 10:
130   if resonators == 0:
131     T_resonators = Tin
132
133   elif resonators == 1:
134     T_resonators = Tin @ T2 @ Tout
135
136   elif resonators == 2:
137     T_resonators = Tin @ T2 @ T1_1 @ T2 @ Tout
138
```

```
  elif resonators == 3:
    T_resonators = Tin @ T2 @ T1_1 @ T2 @ T1_2 @ T2 @ Tout

  elif resonators == 4:
    T_resonators = Tin @ T2 @ T1_1 @ T2 @ T1_2 @ T2 @ T1_3 @ T2 @ Tout

  elif resonators == 5:
    T_resonators = Tin @ T2 @ T1_1 @ T2 @ T1_2 @ T2 @ T1_3 @ T2 @ T1_4 @ T2 @
   Tout

  elif resonators == 6:
    T_resonators = Tin @ T2 @ T1_1 @ T2 @ T1_2 @ T2 @ T1_3 @ T2 @ T1_4 @ T2 @
   T1_5 @ Tout

  elif resonators == 7:
    T_resonators = Tin @ T2 @ T1_1 @ T2 @ T1_2 @ T2 @ T1_3 @ T2 @ T1_4 @ T2 @
   T1_5 @ T2 @ T1_6 @ Tout

  elif resonators == 8:
    T_resonators = Tin @ T2 @ T1_1 @ T2 @ T1_2 @ T2 @ T1_3 @ T2 @ T1_4 @ T2 @
   T1_5 @ T2 @ T1_6 @ T2 @ T1_7 @ Tout

  elif resonators == 9:
    T_resonators = Tin @ T2 @ T1_1 @ T2 @ T1_2 @ T2 @ T1_3 @ T2 @ T1_4 @ T2 @
   T1_5 @ T2 @ T1_6 @ T2 @ T1_7 @ T2 @ T1_8 @ Tout

  elif resonators == 10:
    T_resonators = Tin @ T2 @ T1_1 @ T2 @ T1_2 @ T2 @ T1_3 @ T2 @ T1_4 @ T2 @
   T1_5 @ T2 @ T1_6 @ T2 @ T1_7 @ T2 @ T1_8 @ T2 @ T1_9 @ Tout


  #If more resonators are used this error will be displayed.
  else:
      raise ValueError("Invalid number of resonators. Must be between 0 and 10."
   )


  #Flattening out T to comute the coefficients
  T11, T12, T21, T22 = T_resonators.flatten()
  #Transmission coefficient
  T_coeff = abs((2) / ((T11 + (T12 / Z_v) + T21 * Z_v  + T22)))
  #Reflection coefficient
  R_coeff = abs( (T11 + (T12 / Z_v) - T21 * Z_v  - T22)  / (T11 + (T12 / Z_v) +
   T21 * Z_v  + T22)  )
  #Transmission loss
  TL = 20*np.log10(T_coeff**-1)
  #Absorption coefficient
  absor = 1 - abs(T_coeff)**2 - abs(R_coeff)**2

  return T_coeff, R_coeff, TL, absor


#Cost function
def cf(i, freq, cost_arrays):
  cost_value = (1 / len(freq)) * sum(cost_arrays[i])
  return cost_value
```

C COMSOL

C.1 Parameters

Name	Value	Description
R	0.05 [m]	Radius waveguide
r	0.011176 [m]	Radius resonator
l	0.0437 [m]	Length resonator
l_c	0.9*l	Length resonator cavity
l_n	l - l_c	Length resonator neck
area	pi*r^2	Cross-sectional resonator surface area
Area	pi*R^2	Cross-sectional waveguide surface area
T1	0.2 [m]	Length T_w1
T2	0.2 [m]	Length T_w2
T3	0.2 [m]	Length T_w3
T4	0.2[m]	Length T_w4
T5	0.2 [m]	Length T_w5
T6	0.2 [m]	Length T_w6
T7	0.2 [m]	Length T_w7
T8	0.2 [m]	Length T_w8
T9	0.2 [m]	Length T_w9
T10	0.2[m]	Length T_w10
T11	0.2 [m]	Length T_w11
Lextra	0.3 [m]	Extra length between inlet/outlet and resonator system
ca	343 [m/s]	Speed of sound in air
rho0	1.293 [kg/m^3]	Density of air
Cp	700 [J/kg*K]	Specific heat air
eta	1.81 × 10-5 [kg/(m*s)]	dynamic viscosity air
vis	eta/rho0	kinematic viscosity air
kt	25.87 [mW/m*K]	Thermal conductivity air
Pr	Cp*eta/kt	Prandtl number air
gamma	1.4	Heat capacity ratio
cw	1461 [m/s]	Speed of sound in water
$rho0_w$	998 [kg/m^2]	Density of water
Cp_w	4184 [J/kg*K]	specific heat water
eta_w	1.0016 [mPa*s]	dynamic viscosity water
vis_w	$eta_w/rho0_w$	kinematic viscosity water
kt_w	0.598 [W/m*K]	Thermal conductivity water
Pr_w	$Cp_w * eta_w/kt_w$	Prandtl number water
$gamma_w$	1.330	heat capacity ratio

Table 2: Model parameters

C.2 Tuning Δl

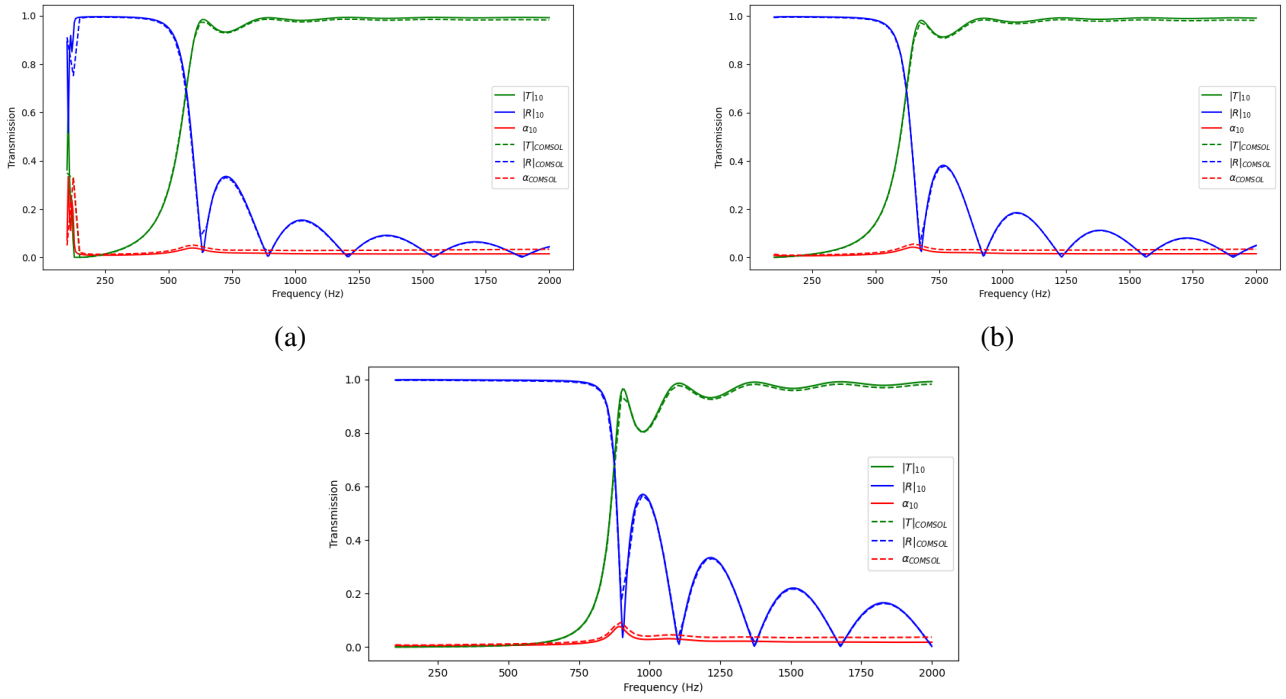

(a) (b)

(c)

Figure 34: Transmission, reflection and absorption for the periodic inhomogeneous system with (a) $l_c = 0.1$ ($\Delta l_t = \Delta l$), (b) $l_c = 0.3$ ($\Delta l_t = \Delta l$) and (c) $l_c = 0.7$ ($\Delta l_t = \Delta l$).